Differential modification of the C-terminal tails of different α-tubulins and their importance for microtubule function *in vivo*

Mengjing Bao, Ruth Dörig, Paula Vazquez-Pianzola, Dirk Beuchle, and Beat Suter

Institute of Cell Biology, University of Bern, Switzerland

Summary

1. α-tubulin glutamylation was established in the C-terminal domain of *Drosophila* αTub84B and αTub84D (αTub84B/D). Multiple glutamyl residues were pinpointed in this domain. The female germline α-tubulin, αTub67C, is, however, not glutamylated.
2. *TTLL5* is required for mono- and poly-glutamylation of αTub84B/D.
3. *TTLL5* is required for the proper Kinesin heavy chain (Khc) distribution in the germline, and the kinesin-based refinement of Staufen localization and ooplasmic streaming during late oogenesis.
4. *TTLL5* is needed for the pausing of anterograde trafficking of mitochondria in axons.

Abstract

Microtubules (MTs) are built from α-/β-tubulin dimers and used as tracks by kinesin and dynein motors to transport a variety of cargos, such as mRNAs, proteins, and organelles, within the cell. Tubulins are subjected to several post-translational modifications (PTMs). Glutamylation is one of them, and it is responsible for adding one or more glutamic acid residues as branched peptide chains to the C-terminal tails of both α- and β-tubulin. However, very little is known about the specific modifications found on the different tubulin isotypes *in vivo* and the role of these PTMs in MT transport and other cellular processes *in vivo*. In this study, we found that in *Drosophila* ovaries, glutamylation of α-tubulin isotypes occurred clearly on the C-terminal ends of αTub84B and αTub84D (αTub84B/D). In contrast, the ovarian α-tubulin, αTub67C, is not glutamylated. The C-terminal ends of αTub84B/D are glutamylated at several glutamyl side chains in various combinations. *Drosophila TTLL5* is required for the mono- and poly-glutamylation of ovarian αTub84B/D and with this for the proper localization of glutamylated microtubules. Similarly, proper kinesin distribution in the

germline also depends on *TTLL5* as well as the refining of Staufen localization and the normal fast ooplasmic streaming with its directional movement, two processes known to depend on kinesin activities. In the nervous system, the pausing of anterograde axonal transport of mitochondria is affected by an enzymatically dead mutant of *TTLL5*. Our results demonstrate *in vivo* roles of *TTLL5* in differential glutamylation of α-tubulins and point to the *in vivo* importance of α-tubulin glutamylation for kinesin-dependent processes.

Introduction

Microtubules (MTs) are fundamental cytoskeletal filaments comprising heterodimers of α- and β-tubulins. Despite their high level of conservation in eukaryotes, MTs are still quite diverse because cells express different tubulin genes and proteins, which can undergo several different post-translational modifications (PTMs). Based mainly on *in vitro* assays, these variants are thought to optimize the MT interaction with different microtubule-associated proteins (MAPs) and motors.

Drosophila melanogaster possesses four α-tubulin genes. Three of them are expressed during oogenesis and early embryogenesis, suggesting that they contribute to the formation of microtubules during these stages. The three genes are *αTub84B*, *αTub84D,* and *αTub67C* (Kalfayan and Wensink, 1982). *αTub84B* and *αTub84D* differ in only two amino acids. Their primary sequence in the C-terminal domain is identical, and both are expressed in most tissues and throughout development. In contrast, *αTub67C* is expressed exclusively during oogenesis, where it is maternally loaded into the egg and embryo. The primary structure of αTub67C is distinctively different from αTub84B/D (Theurkauf et al., 1986). These differences are also apparent in the C-terminal domain and include the last residue, phenylalanine (Phe, F) in αTub67C and tyrosine (Tyr, Y) in αTub84B/D. *αTub85E* is the fourth α-tubulin but is mainly expressed in testes but not in ovaries (Kalfayan and Wensink, 1982).

MTs are subjected to several PTMs, including the C-terminal tail glutamylation, glycylation, and detyrosination / tyrosination. Furthermore, acetylation and phosphorylation in the more central parts of the tubulins have also been identified (Arce et al., 1975; Eddé et al., 1990; Hallak et al., 1977; L'Hernault and Rosenbaum, 1985; Magiera and Janke, 2014; Redeker et al., 1994). Glutamylation is a PTM that adds one or more glutamic acids (Glu, E) to the side chains of glutamic acid residues in the C-terminal tails of both α and β tubulin,

64 causing the formation of a branched peptide chain (Eddé et al., 1990; Redeker et al., 1992).
65 Glycylation is another PTM that adds glycines to the γ-carboxyl group of glutamic acid
66 residues in the C-terminal region (Redeker et al., 1994). At least in vertebrates, tubulin is
67 also subjected to a particular cycle of de-tyrosination-tyrosination (Preston et al., 1979). In
68 this case, the C-terminal Tyr or Phe of α-tubulin is cyclically removed, resulting in a C-
69 terminal Glu residue, and a new Tyr can be re-added to the new C-term. The enzymes that
70 catalyze glutamylation, glycylation, and tyrosination belong to the Tubulin-tyrosine-ligase-like
71 (TTLL) family (Janke et al., 2005). In *Drosophila melanogaster*, this family encompasses 11
72 genes (flybase.org).

73 MTs have an intrinsic polarity with a plus and a minus end. On these tracks, kinesin
74 motors transport cargo to the plus ends, and dynein motors move cargo toward the minus
75 ends. Evidence for the importance of PTMs of tubulin subunits has already been reported *in*
76 *vitro.* Artificial tethering of 10E peptides to the side chains at position E445 of α-tubulin and
77 E435 of β-tubulin by maleimide chemistry increased the processivity (the run length) of
78 kinesin motors on tubulin. For Kinesin-1, this was a 1.5-fold increase (Sirajuddin et al.,
79 2014). In contrast to kinesin, Dynein/dynactin motors preferred a Tyr at the C-term of α-
80 tubulin to initiate processive transport *in vitro* because the motor favored this isotype as an
81 attachment point to dock onto the MTs (McKenney et al., 2016). Recent work now also
82 demonstrated a role for the mouse tubulin glycylation enzymes. *In vitro* fertility assays
83 showed that the lack of both *TTLL3* and *TTLL8* perturbed sperm motility, causing male
84 subfertility in mice. Structural analyses further suggested that loss of glycylation decreased
85 axonemal dynein activity (Gadadhar et al., 2021).

86 *CG31108* is considered to be the homolog of the mammalian *TTLL5* gene and was
87 therefore named *DmTTLL5 or TTLL5* (Devambez et al., 2017). It is required for α-tubulin
88 glutamylation in the *Drosophila* nervous system (Devambez et al., 2017). The murine TTLL5
89 is composed of an N-terminal core tubulin tyrosination ligase-like (TTLL) domain, a cofactor
90 interaction domain (CID), and a C-terminal receptor interaction domain (RID) (Lee et al.,
91 2013). The N-terminal core domain was shown to provide the catalytic activity of TTLL5 and
92 is highly conserved in *Drosophila* TTLL5 (van Dijk et al., 2007, Natarajan et al., 2017) (**Table**
93 **1**). According to the FlyBase data, *Drosophila TTLL5* mRNA is expressed at high levels in
94 ovaries (**Table S1**), even higher than in the nervous system where initial studies were
95 performed (Devambez et al., 2017). We thus focused on *TTLL5*'s possible functions during
96 *Drosophila* oogenesis to shed light on possible *in vivo* roles of glutamylated α-tubulins.

97 A recent *in vivo* mouse study showed that the absence of polyglutamylation of α-tubulin
98 but not β-tubulin increased the overall (both anterograde and retrograde) motility of

99 mitochondria transport in axons (Bodakuntla et al., 2021). However, another study showed
100 that the vesicular axonal transport was not affected by the absence of MT glutamylation in
101 *Drosophila TTLL5* mutant larvae (Devambez et al., 2017). Given these contradictory results,
102 we also studied the function of *TTLL5* in neurons.

103 Our results revealed that *TTLL5* is essential for the normal glutamylation of the ovarian
104 αTub84B/D. Surprisingly, even in wild-type ovaries, the oogenesis-specific aTub67C was not
105 glutamylated, suggesting that this gene, *αTub67C,* may have evolved to produce MTs that
106 contain regions that are less glutamylated. We found that *TTLL5* is required for the normal
107 distribution of kinesin, for proper cytoplasmic streaming during late oogenesis as well as for
108 fine-tuning kinesin-based localization of Staufen protein. Furthermore, *TTLL5* has a clear
109 effect on the pausing of mitochondria during anterograde axonal transport in wing nerves.
110 Our work, therefore, reveals the *in vivo* importance of glutamylation of specific α-tubulins.

111

112 **Results**

113 **Specific glutamylation on multiple Glu residues of αTub84B/D, but not αTub67C in**
114 **ovaries**

115 Mass spectrometry was performed to analyze the glutamylation of the C-terminal tails of α-
116 tubulins *in vivo*. Proteins extracted from ovaries were purified through SDS-PAGE, and α-
117 tubulin bands were cut out and digested with the protease trypsin-N. C-terminal peptides of
118 the different α-tubulin isotypes were then analyzed for post-translational modifications by
119 liquid chromatography-mass spectrometry (LC-MS). Because the resulting C-terminal
120 peptides are identical between the αTub84B and αTub84D, we refer to them as αTub84B/D
121 (**Fig. 1A**). Analyses of wild-type ovarian extracts revealed that the general *Drosophila* α-
122 tubulins αTub84B/D, but not the ovarian-specific αTub67C, showed glutamylation on their C-
123 terminal tails (**Fig. 1A**). For αTub84B/D, side chain glutamylation was identified on all four
124 glutamyl residues in the tail region, Glu443, Glu445, Glu448, and Glu449. The most
125 extended side chains identified were 3Es in wild-type ovaries **(Fig. 1A,1B)**. According to
126 FlyBase, *αTub84B+D* mRNAs are 4.7x as highly expressed as *αTub67C*. We identified a
127 similar ratio (4.6x) of C-terminal peptides by the MS analysis (**Table S2**). Because of the
128 lower abundance of Tub67C C-terminal peptides, we cannot rule out that rare glutamylation
129 on the maternal αTub67C exists. Altogether, we conclude that glutamylation of α-tubulin had
130 a strong preference for the C-terminal domain of αTub84B/D.

131 ***Drosophila TTLL5* is required for MT mono- and polyglutamylation of ovarian**
132 **αTub84B/D.**

133 To study the function of TTLL5, distinct *TTLL5* loss-of-function mutations were created and
134 characterized (**Fig. 2A**). The *TTLL5*^{pBac} and *TTLL5*^{Mi} mutant strains carry a piggyBac and a
135 Minos transposon, respectively, within the open reading frame of *TTLL5*. The *TTLL5*^{MiEx}
136 mutant was generated by imprecise excision of the Minos element, which caused the
137 formation of a premature stop codon at gene position 8,132 in the open reading frame
138 (codon position 392). An anti-TTLL5 antibody that cross-reacts with additional proteins in
139 ovarian extracts also recognized a band corresponding to the calculated mass of TTLL5.
140 This band was absent in ovarian extracts prepared from the three *TTLL5* mutants,
141 suggesting that they are protein nulls for *TTLL5* or make only a truncated protein (**Fig. 2B**).
142 A transgene containing the wild-type *Drosophila TTLL5* sequence fused to the Venus
143 fluorescent protein sequence under UAS control (UASP-*Venus::TTLL5*) was also produced
144 as a tool to rescue the phenotypes produced by the *TTLL5* mutations and for overexpression
145 studies (**Fig. 2A**).

146 To quantify the effect of *TTLL5* on the glutamylation of the C-terminal tails of α-tubulins,
147 we determined the frequency of C-terminal peptides containing the entire primary sequence
148 and 0, 1, 2, or 3 Glu (E) modifications. This analysis was performed with extracts from wild-
149 type ovaries and the different *TTLL5* mutant ovaries. Wild-type ovaries revealed that 62% of
150 the peptides were modified, 41% with 1E, 14% with 2Es, and 7% with 3Es **(Table 2)**. On the
151 other hand, no glutamylation was observed in *TTLL5*^{pBac} and *TTLL5*^{MiEx} mutants. This clearly
152 shows that *Drosophila TTLL5* is essential for the side chain glutamylation of the C-terminal
153 Glu443, Glu445, Glu448, and Glu449 of αTub84B/D.

154 We also measured the levels of monoglutamylation of α-tubulin by western blotting using
155 the GT335 antibody. This antibody reacts with the first glutamate on the glutamate side-
156 chain even if it is polyglutamylated (**Fig. 3A**) (Wolff et al., 1992). Note that the GT335
157 antibody does not reliably detect all mono glutamylated residues in *Drosophila* tubulins
158 because GT335 preferentially recognizes the first Glu attached to a Glu residue in an acidic
159 environment. In mice, the middle Glu in the sequence -G**E**E- of the C-terminal tail of α-
160 tubulin is such an "acidic" site. Once glutamylated, the branched Glu modification can be
161 recognized by GT335 (Bodakuntla et al., 2021). In contrast, in *Drosophila* α-tubulin, both
162 E443 and E445 in the sequence -G**E**G**E**G- are flanked by Glycines on both sides, which
163 does not provide the acidic environment needed for efficient recognition by GT335. The
164 GT335 signal may, therefore, mainly stem from the glutamylation on the consecutive Glu
165 residues E448 and E449 in the sequence -GA**EE**Y. On Western blots from wild-type

166 extracts, the GT335 antibody produced a band at the expected position, and this band was
167 reduced in all *TTLL5* mutants **(Fig. 3B)**. The GT335 signals were restored and even
168 increased in some *TTLL5* mutants upon overexpression of the rescue construct
169 *Venus::TTLL5*, showing that the signal is specific and can be used to monitor *TTLL5* activity.
170 We conclude that *TTLL5* is required for the monoglutamylation of α-tubulin.

171 The 1D5 antibody recognizes α-tubulin with an -XEE sequence at the C-terminal α-
172 carboxylate group (with X being a variable residue) (Rüdiger et al., 1999) **(Fig. 3C)**.
173 Therefore, in principle, all Glu residues E443, E445, E448, E449, and the C-terminal Glu
174 residues E448/449 can be recognized if they are not followed by another amino acid (such
175 as Tyr) at their α-carboxylate group. 1D5 does not cross-react with C-terminal Glu residues
176 E448/449 in tyrosinated α-tubulin. Because *w* control ovaries showed high 1D5 cross-
177 reactivity with a polypeptide of the predicted size, this, therefore, indicates the presence of
178 glutamate side chains containing at least two glutamates and possibly C-terminally de-
179 tyrosinated α-tubulin (Gadadhar et al., 2017; Preston et al., 1979) **(Fig. 3D)**. Consistent with
180 the MS analysis, the *TTLL5* mutants showed a strongly reduced signal with 1D5, indicating
181 that loss of *TTLL5* function prevents normal polyglutamylation. The 1D5 signal was again
182 restored in all *TTLL5* mutants upon expression of the rescue construct. Overexpression of
183 TTLL5 in $TTLL5^{pBac}$ and $TTLL5^{Mi}$ even produced a stronger 1D5 signal and an up-shifted
184 band, suggesting that α-tubulin gets hyperglutamylated **(Fig. 3D)**. These results reveal that
185 *TTLL5* is essential for the glutamylation of the α-tubulin subunit. The result that the rescue
186 construct induced the appearance of hyperglutamylated α-tubulin also suggests that, in
187 normal cases, the endogenous TTLL5 levels are usually limiting in ovaries.

188 Most of the murine TTLL5 residues involved in α-tubulin glutamylation (Natarajan et al.,
189 2017) are conserved in *Drosophila* TTLL5 **(Table 1;** Natarajan et al., 2017**)**. Two are known
190 to be essential for the general enzymatic activity of TTLLs, and two for the interaction with
191 the C-terminal domain of α-tubulin **(Fig. 3E)**. To determine whether these residues are
192 indeed needed *in vivo* for the enzymatic activity of *Drosophila TTLL5* towards αTub84B/D,
193 we used CRISPR/Cas9 to mutate the conserved codons in *Drosophila TTLL5. Drosophila*
194 TTLL5 residues K282 and E517 correspond to mouse K131 and E336*,* respectively*.* They
195 directly interact with ADP/ATP and thus affect general TTLL5 enzymatic activity (Natarajan
196 et al., 2017). $TTLL5^{R339}$ corresponds to mouse $TTLL5^{R188}$*,* which is vital for TTLL5's
197 glutamylation activity. $MmTTLL5^{R188}$ resides in the β6-7 loop, which forms a salt-bridge
198 interaction with the C-terminal tail of α-tubulin and orients it towards the ATP/ADP-binding
199 site (van Dijk et al., 2007). Glutamylation of α-tubulin was impaired in all these *TTLL5*
200 mutants where the conserved residue was replaced **(Fig. 3F)**. Since these mutations did not

201 abolish the stability of the corresponding mutant protein (**Fig. S1**), our results revealed the
202 importance of E517, K282, and R399 of *Drosophila* TTLL5 for glutamylation. Most active site
203 residues of human TTL (Prota et al., 2013; van Dijk et al., 2007) are also conserved between
204 mammalian and *Drosophila* TTLL5 **(Table 3)**. We also mutated the *Drosophila TTLL5*^{P522}
205 codon corresponding to human *TTL*^{P336} (and human *TTLL5*^{P371}/mouse *TTLL5*^{P371}), which is
206 required for anchoring TTL to α-tubulin by forming hydrogen bonds with C-terminal tail
207 residues of α-tubulin (Prota et al., 2013). However, the importance of *TTLL5*^{P371} for
208 glutamylation has not been reported in mammalian systems. Surprisingly, P522 turned out to
209 be essential for glutamylation, revealing P522 as a novel critical residue for the glutamylation
210 function of TTLL5. We also tested whether the overexpression of *TTLL5* in a wild-type
211 background affected polyglutamylation similarly. Indeed, *UASP-Venus::TTLL5*
212 overexpression in ovaries led to hyperglutamylation, as evident from the stronger signal and
213 the additional upshifted band **(Fig. 3G).** All these results point to *TTLL5's* essential role in
214 the glutamylation of α-tubulin.

215 **Other PTMs of the C-terminal tail of ovarian α-tubulin**

216 Western blotting showed no or only minor changes in tyrosinated α-tubulin levels in any of
217 the null or CRISPR/Cas9 generated point mutants, and *TTLL5* overexpression did also not
218 affect these levels **(Fig. 3B, 3F, 3G).** TTLL5 levels, therefore, do not appear to affect levels
219 of tyrosinated α-tubulin in ovaries.

220 Our MS results also detected glycylated C-terminal α-tubulin peptides in ovarian samples.
221 Such glycylations were observed in αTub84B/D but not in αTub67C **(Fig. S2A, S2B)**. Up to 2
222 glycines were primarily detected on Glu443, Glu445, Glu448, or Glu449 of αTub84B/D. The
223 frequency of C-terminal peptides containing Gly (G) modifications was similar or somewhat
224 higher in *TTLL5* mutants compared to the wild-type control **(Fig. S2C)**, suggesting that
225 *TTLL5* is not needed for this modification or even counteracts it.

226 **Presence of polyglutamylated microtubules in ovaries**

227 We then analyzed the distribution of polyglutamylated microtubules during oogenesis by
228 immunofluorescence using the 1D5 antibody. Specific 1D5 immunofluorescence signals
229 were observed in the follicle cells and oocytes throughout the previtellogenic, middle, and
230 late oogenesis stages (**Fig. 4**). In the stage 10B (S10B) oocyte, the 1D5 signal showed a
231 slightly biased localization in the cortical region of the oocyte. We observed a robust
232 reduction of the 1D5 signal in *TTLL5* mutant ovaries, revealing that *TTLL5* is essential for the

233 appearance of polyglutamylated microtubules in the ovaries and their concentration at the
234 oocyte cortex in S10B.

235 **Effect of *TTLL5* on the refinement of posterior localization of Staufen**

236 *osk* mRNA localization, combined with translation control, is essential for targeting Osk
237 protein expression to its proper posterior compartment in the cell during mid and late
238 oogenesis (Weil, 2014). Staufen is a protein that associates with *osk* mRNA into a
239 ribonucleoprotein (RNP) complex during *osk* mRNA localization. It therefore also serves as a
240 proxy for *osk* mRNA localization. Staufen/*osk* mRNA localization requires the
241 dynein/dynactin-mediated minus-end transport machinery in the early stages of oogenesis.
242 Subsequently, the Staufen/*osk* mRNA becomes localized to the posterior of the oocyte from
243 the mid to late stages of oogenesis. This particular Staufen/*osk* mRNA localization phase
244 within the oocyte depends on kinesin-driven processes including active transport and
245 ooplasmic streaming in S10B oocytes (Kato and Nakamura, 2012; Lu et al., 2018; Brendza
246 et al., 2000; Zimyanin et al., 2008).

247 To determine whether *TTLL5* contributes to these processes, we studied the role of
248 *TTLL5* in the localization of Staufen in ovaries lacking functional TTLL5. In the wild type,
249 the localization of Staufen appeared very tight on the cortex with little lateral
250 extension in S10B (**Fig. 5A**). In ovaries lacking functional TTLL5, we observed a
251 more diffuse localization pattern of Staufen in the S10B egg chambers of all *TTLL5*
252 null mutants (**Fig. 5B**). Z-stack images revealed a more diffusely spread Staufen signal in
253 the *TTLL5* null mutants, although this varied more between different samples. The increased
254 length of the crescent was fully reversed to the regular length in all UAS-*Venus::TTLL5*
255 rescued strains **(Fig. 5C)**. These results suggest that *TTLL5* is required for tight cortical
256 accumulation of Staufen in S10 oocytes. We also analyzed the distribution of Venus::TTLL5
257 during oogenesis. Antibody staining suggested that Venus::TTLL5 strongly accumulated in
258 the oocyte, especially along the cortex **(Fig. 5C)**. To exclude possible artifacts of the
259 antibody staining, we also tried to observe the self-fluorescent of the Venus tag. Though the
260 Venus fluorescence was relatively weak, Venus::TTLL5 also showed a cortical preference in
261 S10B oocytes, similar to that found by antibody staining (**Fig. S3**). This stronger cortical
262 accumulation of Venus::TTLL5 coincides also with the region where polyglutamylated
263 microtubules were enriched at the same stage **(Fig. 4)**.

264 In the *TTLL5* point mutants, where specifically the enzymatic activity of TTLL5 was
265 blocked ($TTLL5^{E517A}$, $TTLL5^{P522A}$, $TTLL5^{R339A}$) the localization pattern of Staufen was not

266 refined and the Staufen signal remained less tightly focused (**Fig. 5D**). An established
267 method to quantify the localization of Staufen to the posterior cortex is to measure the length
268 of the posterior Staufen crescent along the cortex (Lu et al., 2016). A shorter crescent is a
269 sign of tighter localization. Indeed, we found that the length of the posterior Staufen crescent
270 was significantly increased in *TTLL5* null and *TTLL5* point mutant ovaries compared to the
271 control and UAS-*Venus::TTLL5* rescued ovaries (**Fig. 5E)**.

272 We did not observe clear differences in Staufen distribution between the wild type and
273 *TTLL5* mutants in S9 and earlier, previtellogenic stages of oogenesis (**Fig. 5F**). Altogether,
274 these results suggest that the requirement for *TTLL5* for tight cortical accumulation of
275 Staufen starts around S10 and the proper refinement of Staufen localization requires
276 glutamylation of α-tubulin.

277 **The onset of fast ooplasmic streaming requires *TTLL5***

278 Ooplasmic streaming is a process that contributes to the refinement of the posterior
279 localization of Staufen (Lu et al., 2016). It is a bulk movement of the oocyte cytoplasm that
280 circulates and distributes mRNAs and proteins in the oocyte, including the Staufen/*osk*
281 mRNA RNPs. It allows these mRNAs and proteins to reach their intended position, where
282 they become anchored. Ooplasmic streaming can be observed in the mid-stage to the late-
283 stage oocytes. Slow and nondirectional flows initiate at stages 8–9 and are followed by rapid
284 and circular streaming at S10B (Lu et al., 2016). The onset of the fast streaming phase has
285 so far been reported to be attributed to 1) microtubule sliding between stably cortically
286 anchored microtubules and free cytoplasmic microtubules close to the cortex (Lu et al.,
287 2016) and 2) subcortical dynamic microtubule-mediated cargo transport (Monteith et al.,
288 2016). Because the final posterior localization refinement of Staufen in S10B oocytes
289 depends on fast streaming (Lu et al., 2016) and also *TTLL5*, we thus wanted to determine if
290 *TTLL5* contributes to fast ooplasmic streaming.

291 We followed the streaming flow in real time by measuring vesicle movement in DIC time-
292 lapse movies (**Mov. S1-S5**). We then tracked the movement of the vesicles along the cortical
293 region where microtubule sliding and transport occur (**Fig. 6A, 6B**). The analysis of the
294 kymographs of these tracked vesicles showed that almost all 24 control ovaries had a typical
295 streaming pattern and that the vesicles were moving unidirectionally parallel to the cortex.
296 However, $TTLL5^{MiEx}$ and $TTLL5^{E517A}$ mutant ovaries displayed abnormal streaming patterns.
297 These abnormal streaming patterns included a partial disruption of streaming especially in
298 the posterior part of the oocyte and a disordered streaming flow in the oocyte (**Fig. 6C**). The
299 typical streaming pattern was restored in $TTLL5^{MiEx}$ ovaries expressing a *Venus::TTLL5*

300 rescue construct. We also evaluated streaming flows in oocytes overexpressing
301 *Venus::TTLL5.* The higher level of TTLL5 did not seem to severely alter the streaming. We
302 thus conclude that the onset of fast streaming in S10B oocytes requires *TTLL5*. Again,
303 because abnormal streaming was observed when the enzymatic glutamylation activity of
304 TTLL5 was impaired (*TTLL5*^{E517A}), our results suggest that TTLL5 acts on the ooplasmic
305 streaming through its role in MT glutamylation.

306 ***TTLL5* affects kinesin distribution in the late-stage female germline**

307 Both Staufen/*osk* mRNA localization and ooplasmic streaming depend on kinesin-driven
308 processes (Serbus et al., 2005)(Brendza et al., 2000). We, therefore, examined whether
309 *TTLL5* somehow affects kinesin. The levels of ovarian Kinesin heavy chain (Khc) were
310 neither affected by lack of *TTLL5* function (**Fig. 7A**) nor by *TTLL5* overexpression (**Fig. 7B**).
311 Next, we determined the localization of Khc in stage 10B, when the fast streaming starts.
312 Even though the MT arrays start to disassemble and re-organize in the S10B oocyte, Khc
313 showed a biased enrichment at the posterior in most of the oocytes in the wild-type control
314 (**Fig. 7C**). Out of 37 wild-type oocytes, 76% showed a posteriorly enriched Khc signal (**Fig.
315 7D**). In contrast, Khc distribution showed a posterior oocyte enrichment in only 13% and
316 14%, respectively, in *TTLL5*^{pBac} and *TTLL5*^{MiEx} mutant egg chambers, respectively (**Fig. 7C
317 and 7D**). Surprisingly, higher expression of *TTLL5* also led to fewer oocytes (54%) showing
318 a posterior Khc enrichment (**Fig. 7C and 7D**). These results demonstrate that moderate
319 levels of *TTLL5* are needed for the proper posterior enrichment of Khc in S10B oocytes.

320 Khc also showed higher accumulation in the interior of the wild-type oocyte (arrowhead in
321 **Figs. 7C, 7E, and 7G**) and this was seen in 76% of the oocytes (**Fig. 7F**). We measured the
322 fluorescence intensity of the Khc signal along the anterior-posterior (AP) axis of the oocytes
323 (line in **Fig. 7E).** In wild-type ovaries, the signal intensity showed a peak in the middle part of
324 the AP axis (**Fig. 7G**), indicating that Khc concentration is higher in the central region of the
325 oocyte. It is worth noting that in the wild-type control, the peaks did not always appear in the
326 middle of the AP line (**Fig. S4**), indicating that Khc concentration can increase in different
327 locations in the inner part of the oocyte. In the *TTLL5* mutants, the inner accumulation of Khc
328 was strongly reduced or absent (**Fig. 7E, 7G, S4**). Only 19% of *TTLL5*^{pBac} and 14% of
329 *TTLL5*^{MiEx} oocytes showed a slight Khc accumulation (**Fig. 7F**). Overexpressing TTLL5 in
330 wild-type oocytes showed an inner peak of Khc accumulation in only 65%, which is slightly
331 less than the wild-type control. Interestingly, the higher levels of TTLL5 sometimes led to two
332 peaks of internal Khc accumulation in the oocyte (**Fig. 7E**, **7G, and S4**). These results show
333 that *TTLL5* activity affects the proper distribution of Khc in the S10B oocytes and they

334 suggest that the inner accumulation of Khc might be causally connected to the circular
335 movement of the fast cytoplasmic streaming.

336 We also evaluated the localization of the Bicaudal-D (BicD) protein during the early stages
337 of oogenesis. BicD is the linker that couples diverse cargos to the dynein/dynactin motor and
338 can thus serve to evaluate dynein transport (Claussen and Suter, 2005). The expression
339 levels of BicD were not affected by the TTLL5 levels (**Fig. S5A**). Also, BicD localized to the
340 posterior of the oocytes, and the ratio of the oocytes showing posteriorly localized BicD was
341 similar in controls and *TTLL5* mutants (**Fig. S5B and S5C**). In conclusion, these results
342 indicated that in oocytes, fully normal kinesin distribution during late stages requires *TTLL5*.
343 In contrast, dynein localization in early oogenesis does not appear to depend on *TTLL5*.

344 **Female fertility and ovarian development do not require *TTLL5***

345 The dramatic loss of polyglutamylated ovarian α-tubulin and the phenotypes during late
346 oogenesis in *TTLL5* mutants incited us to analyze whether the morphology of the egg
347 chambers from different stages and female fertility were affected in *TTLL5* mutants.
348 However, the lack of *TTLL5* neither caused a significant decrease in hatching rates, nor
349 distinguishable morphological changes in ovaries.

350 **The glutamylation activity of *TTLL5* modulates the pausing of anterograde axonal**
351 **transport of mitochondria**

352 Previous studies in *Drosophila* reported that the absence of α-tubulin glutamylation did not
353 seem to be detrimental to the nervous system functions tested in *Drosophila* (Devambez et
354 al., 2017). The wing nerve is an additional, attractive system to monitor organelle transport,
355 such as the movement of mitochondria (Vagnoni and Bullock, 2016) (Hollenbeck and
356 Saxton, 2005). We thus used wing nerves to study the role of *TTLL5* and glutamylation for
357 neuronal transport in the peripheral nervous system by tracking the movement of GFP-
358 labelled mitochondria (Mito::GFP) in the arch of the L1 region which contains bundles of
359 axons (Vagnoni and Bullock, 2016) (**Fig. 8A**). The mitochondria transported towards the
360 thorax (to the right) move by plus-end transport, which is driven by kinesin, whereas
361 mitochondria transported oppositely are transported by dynein (Vagnoni and Bullock, 2016).
362 Time-lapse videos of Mito::GFP movements are shown in **Mov. S6**. Mitochondria are usually
363 transported unidirectionally over a 3 min tracing time. Bidirectionally moving particles were
364 seen, but only rarely. In these cases, they usually moved a short distance toward one
365 direction, suddenly turned back, and ran in the opposite direction. A schematic running
366 pattern is shown in **Fig. 8B.** The start of a run was chosen at the time point when a motile

367 particle began to move away from a stationary position or when it entered the focal plane,
368 and the stop of a run was set when the particle terminated moving or moved out of the focal
369 plane in the given time window. The “pausing” was called when the particle moved at a rate
370 lower than 0.2 μm/s within the time window of a “run”. Particles with speeds higher than 0.2
371 μm/s were considered “trafficking”. Motile mitochondria were manually tracked in both
372 anterograde and retrograde directions. For the anterograde transport, the run length of
373 mitochondria was similar for each “run” between wild-type controls and *TTLL5*^{E517A} (**Fig. 8C**).
374 However, a significant increase was observed in the net velocity in *TTLL5* ^{E517A} compared to
375 wild-type controls (**Fig. 8D**). We investigated the reason and found that the absence of
376 enzymatically active *TTLL5* did not alter the trafficking velocity of mitochondria (**Fig. 8E**), but
377 dramatically decreased the total pausing time (1.4 times less) of the anterograde transport of
378 mitochondria (**Fig. 8F**). This suggested that *TTLL5* might not directly affect the trafficking but
379 rather the pausing of mitochondrial transport. To further study the pausing behavior of
380 mitochondria, kymographs of individual motile mitochondria were generated. Kymographs of
381 three anterograde transported mitochondria are shown for both genotypes (**Fig. 8G**). The
382 pausing of the mitochondria is pointed out by yellow arrowheads. More frequent pausing was
383 observed in controls compared to the *TTLL5*^{E517A}. By analyzing the pausing number in the
384 given distance, we identified a 1.5 times more frequent pausing in controls compared to the
385 *TTLL5*^{E517A} mutant (**Fig. 8H**). These results indicate that the longer total pausing time in
386 controls was most likely due to more frequent pausing during anterograde transport. The
387 effect of the lack of TTLL5 enzymatic activity on retrograde transport was less clear because
388 we did not observe significant differences measuring the parameters of the retrograde
389 transport. To sum up, these results suggest that the glutamylation activity of TTLL5 is
390 needed for controlling the pausing of this anterograde axonal transport.

391

392 **Discussion**

393 **PTMs of the C-terminal tail of ovarian α-tubulin**

394 Side chain glutamylation of the C-terminal domain of α-tubulin in *Drosophila* ovaries was
395 observed using specific antibodies and MS identification. Results from wild-type ovaries and
396 mutants revealed that *TTLL5* is essential for these modifications. Consistent with results
397 from mammalian cells and the *Drosophil*a nervous system (Devambez et al., 2017; van Dijk
398 et al., 2007), the complete lack of monoglutamylated tubulin tails in the presumptive null
399 mutants of *TTLL5* strongly suggests a requirement for *TTLL5* for adding the first branching
400 Glu to the Glu side chains in the C-term. The robust reduction of polyglutamylated tubulin in

401 *TTLL5* mutants found in ovaries and the nervous system (Devambez et al., 2017) further
402 shows that *TTLL5* is also needed, directly or indirectly, for polyglutamylation in *Drosophila.*
403 Mammalian TTLL5 is considered to be an initiator glutamylase and TTLL6 an elongator of
404 polyglutamylation of α-tubulin (Gadadhar et al., 2017). This appears to be different in
405 *Drosophila* ovaries because according to Flybase data, *TTLL6A* and *TTLL6*B are not
406 expressed in ovaries **(Table S1)** and only a surprisingly small fraction of the *TTLL* gene
407 family members is expressed. Aside from *TTLL5*, we only found evidence for the expression
408 of *TTLL4A* and *TTLL12* **(Table S1)**. The predicted mouse homolog of the *Drosophila*
409 *TTLL4A* glutamylates β-tubulin (Mahalingan et al., 2020). The function of the mammalian
410 *TTLL12* is poorly studied and its core TTL domain is less conserved than other mouse E-
411 and G- ligases of the TTLL family (van Dijk et al., 2007). It, therefore, seems possible that
412 *Drosophila* TTLL5 itself might also provide the activity to extend the oligo-Glu side chains. A
413 possibility that cannot easily be tested *in vivo*.

414 The presence of polyglycylated α-tubulin in ovaries (**Fig. S2**) was unexpected because
415 the known *Drosophila* polyglycylases (TTLL3A/B) are not expressed in ovaries (Rogowski et
416 al., 2009) (**Table S1**). Finding that *TTLL5* is not required for this modification in ovaries, it will
417 be interesting to find out if TTLL4A, TTLL12, or other unknown enzymes perform the
418 glycylation of α-tubulin in ovaries.

419 The MS results revealed that glutamylation and glycylation strongly preferred the
420 substrate αTub84B/D over αTub67C, even though αTub67C is an ovarian-specific α-tubulin.
421 This points to a possible need for a side-chain modification resistant α-tubulin in the germline
422 to regulate different transport processes by providing local MT sites with reduced sidechain
423 glutamylation, possibly to allow for longer processive movement of kinesin motors as was
424 observed in the absence of glutamylation in the mitochondrial transport assay **(Fig. 8)**.. It will
425 be interesting to find out whether MT tracks containing specific hypoglutamylated regions
426 exist in oocytes and whether these perform an important function in large insect oocytes that
427 use rapid cytoplasmic streaming to localize patterning factors.

428 Glycylation and glutamylation are found at the same sites in the C-terminal tail of α-
429 tubulin, and glutamylation seems not to be a prerequisite for glycylation. This provokes the
430 question of whether glycylation even serves to prevent glutamylation or competes with it and
431 whether this is used as another level of control of microtubule activity. In *Tetrahymena*, such
432 a competition has been described. There, Glutamic acid and Glycine ligases competed
433 for the same sites or affected each other by sterically blocking adjacent sites of tubulins

434 (Redeker et al., 2005; Wloga et al., 2009). It seems possible that such competition also
435 exists in fly ovaries.

436 **Glutamylation of microtubules and its functions in late-stage oocytes**

437 The cortical concentration of glutamylated MTs in the oocyte arouse our interest in
438 investigating the function of MT glutamylation during oogenesis. In stage 10B, it coincides
439 with the *TTLL5* requirement for the tight posterior localization of Staufen protein and the
440 rapid ooplasmic streaming that contributes to the tighter localization of Staufen. It thus
441 appears that glutamylation of MTs is needed for the rapid ooplasmic streaming and through
442 this process for the localization of Staufen. So far, two kinesin-driven processes are
443 considered to be the driving forces for the rapid ooplasmic streaming. MT sliding between
444 stable cortical MTs and cargo transport on subcortical MTs (Lu et al., 2016) (Monteith et al.,
445 2016). This coincides with our findings that glutamylated microtubules and TTLL5 are slightly
446 more enriched in this cortical region in S10 (**Fig. 4** and **Fig. 5C**), which appears to be a
447 prerequisite for the concentration of Khc in the cortical region (**Fig. 7C**). From this, we
448 propose that glutamylation of the cortical MTs by TTLL5 promotes the kinesin-dependent
449 MT-based processes in the cortical region, leading to rapid ooplasmic streaming and tight
450 posterior localization of Staufen, a process that contributes to defining the posterior pole of
451 the oocyte and egg.

452 **Role of glutamylation of α-tubulin for anterograde axonal transport of mitochondria**

453 The previous study showed that α-tubulin was the only tubulin subunit that can be
454 glutamylated in the *Drosophila* nervous system and *TTLL5* is required for α-tubulin
455 glutamylation in the neurons (Devambez et al., 2017). However, the absence of *TTLL5* did
456 not reveal clear defects in larval neuromuscular junction morphology, larval locomotion
457 behavior, or vesicular axonal transport in larval neurons. We, therefore, used a different
458 system, the transport of mitochondria in the adult wing axon to test for a possible function.
459 This revealed that pauses occurred at higher frequencies during anterograde transport of
460 mitochondria when there was enough active *TTLL5*. This might indicate that the
461 glutamylated side chains of α-tubulin act as marks or even obstacles that break or disturb
462 the anterograde movement of mitochondria. Aside from the peptide side chains, the
463 considerable negative charge of these modified regions **(Fig. 1B)** could contribute to this.

464 The previous *Drosophila TTLL5* study mentioned a slight effect on pausing of vesicles
465 during axonal transport in *TTLL5* mutants had also been noted but turned out to be not
466 significant (Devambez et al., 2017). On the other hand, a recent study revealed a similar

467 function of glutamylation of α-tubulin for the transport of mitochondria. The absence of
468 glutamylation of α-tubulin increased the motility of mitochondria in the mouse neurons but
469 did not affect their transport velocity. The results led to their hypothesis that glutamylation of
470 α-tubulin may not directly affect transport but rather affect mitochondrial docking and motor
471 binding to MT tracks by acting as roadblocks on the MT tracks (Bodakuntla et al., 2021). An
472 additional comparison with this study is worth mentioning. The mammalian study found that
473 the motility of both anterograde and retrograde transported mitochondria was strengthened
474 in the absence of glutamylation of α-tubulin. While our *Drosophila* results showed a selective
475 effect on mitochondrial motility in plus-end transport. This difference might be due to the
476 different modification patterns of the C-terminal part of α-tubulin in mammals and *Drosophila*.
477 In the mammalian system, only one site can be glutamylated but up to 5 Glus can be added
478 as a side chain on an individual tail (Redeker et al., 1992). In *Drosophila* ovaries, the
479 glutamylated side chains are shorter with up to 3 Glus, but often more than one side chain
480 was found on the same C-terminal domain (**Fig. 1B**). It is conceivable that these different
481 modification patterns alter the physical properties of tubulins such that they affect motors
482 and cargos in different ways.

483 Recent studies showed that the recruitment of a microtubule severing protein Katanin to
484 microtubules was enhanced by the α-tubulin tail glutamylation in *C. elegans* (Szczesna et
485 al., 2022). Thus, the glutamine residues on tubulins might regulate the pausing of the axonal
486 transport either by acting as a roadblock on MT tracks or by recruiting severing protein (e.g
487 katanin) that interrupts the MT tracks. Several mechanisms have been identified to stop
488 mitochondrial transport in neurons by interfering with Kinesin-1. For instance, blocking the
489 binding of Kinesin-1 to MTs by increasing Ca^{2+} (Wang and Schwarz, 2009) or abolishing the
490 interaction between Kinesin-1 and mitochondria by degrading one of the linker proteins, Miro
491 (Wang et al., 2011). The *in vitro* studies demonstrated that the artificial tethering of glutamyl
492 peptides to the side chains of MTs affected the function of Kinesin-1 (Sirajuddin et al., 2014).
493 Combined with our studies in oocytes that connected MT glutamylation with kinesin
494 localization and kinesin-driven processes, we suggest that the stop of the mitochondrial
495 transport by tubulin glutamylation in the neurons is caused by stopping kinesin-1.

496 **Physiological relevance of α-tubulin glutamylation**

497 Though without strong physiological defects in flies, our observations still revealed clear
498 functions of tubulin glutamylation for MT motor-based processes *in vivo.* Even though an
499 essential function of α-tubulin glutamylation has not emerged from this study, it has become
500 clear that kinesin-dependent processes are modified or controlled by this modification and
501 that evolution has adapted the tubulin code to optimize the usage of MTs for different

502 evolving needs. That *TTLL5* is not essential for survival also makes this protein an
503 interesting candidate for drugs that can modulate its glutamylation activity to regulate and
504 possibly increase MT transport in neurodegenerative diseases where MT transport is known
505 to be affected.

506

507 **Materials and methods**

508 ***Drosophila* genetics**

509 The fly stocks used in this study, MattubGal4 (7062), *TTLL5*^{pBac} (16140), *TTLL5*^{Mi} (32800),
510 and *Df(3R)BSC679* (26531), were obtained from the Bloomington Drosophila stock center.
511 The *TTLL5*^{MiEx} mutation was made by imprecise excision of the Minos element, which left a
512 3-base insertion (CTA), which introduced a premature stop codon at the genomic position
513 8,132 in the open reading frame (polypeptide position 392). The different *TTLL5* point
514 mutations were generated by CRISPR/Cas9. The two *Drosophila* stocks used for *TTLL5*
515 gene editing, *y[1] M{w[+mC]=nos-Cas9.P}ZH-2A w[*]* and *y[1] v[1] P{y[+t7.7]=nos-*
516 *phiC31\int.NLS}; P{y[+t7.7]=CaryP} attP40* were obtained from the Bloomington *Drosophila*
517 Stock Center (54591) (Port et al., 2014) and (25709), respectively. Target sequences near
518 the K131, R339 R376, and E517 codons were selected to introduce INDELs and the
519 following point mutations: K131A, R339A (b6-7 loop), R376A, and E517A. Phosphorylated
520 and annealed primers (**Table S3A**) needed to construct the corresponding coding
521 sequences for a single guide RNA (sgRNA) were each cloned into the BbsI site of *pCFD5*
522 according to the protocol published on www.crisprflydesign.org. After amplifying the vector in
523 XL1 blue cells, the plasmids were sequenced to verify the correct assembly. Subsequently,
524 they were injected into *attP40* embryos. TTLL5-guide stocks with integrated genes encoding
525 sgRNAs were established *(=v; attP40{v*$^{+}$*, TTLL5-guide}/CyO*). To obtain INDELs for TTLL5,
526 a three-generation crossing schema was set up. Firstly, *nos-cas9* virgins were crossed with
527 males from the different TTLL5-guide stocks. Secondly, the subsequent single male progeny
528 was crossed with *w; Ly/TM3, Sb* virgins. Thirdly, resulting in single *TM3, Sb* males were
529 again crossed with *w; Ly/TM3, Sb* virgins to establish the stocks. The nature of the mutated
530 *TTLL5* gene in each stock was determined by sequencing. To introduce specific point
531 mutations in the *TTLL5* gene, embryos from a cross with *y w {w*$^{+}$*, nos-cas9}* virgins and
532 TTLL5-guide males were injected with the appropriate template (**Table S3B).** The resulting
533 individual adult males were crossed with *w; Ly / TM3, Sb* virgins, and stocks were
534 established. A mutated *TTLL5* gene was confirmed by restriction digestion and subsequent
535 sequencing. All the *TTLL5* alleles were crossed to *Df(3R)BSC679* to test the effect of the
536 *TTLL5* mutations in hemizygous animals. (Abnormally shaped egg chambers were seen in
537 *TTLL5*^{pBac}*/Df(3R)BSC679.* But the phenotype disappeared when in combination with specific
538 2nd chromosomes, for example, *MattubGal4/+ or +/UAS-Venus::TTLL5).* The *UASp-*
539 *venus::TTLL5* DNA construct was made from the *TTLL5* cDNA amplified by PCR (forward
540 primer: 5′ - GTTCAGATCTATGCCTTCTTCATTGTGTG -3′; reverse primer: 5′ -
541 GAGTCATTCTAGAGCTTCATAGAAATACCTTCTCC- 3′) and inserted into the *pUASP-*

542 *venus* vector via Xba I/Bgl II ligation. DNA was inserted into the *attP-58A* landing platform
543 (24484) to generate the transgenetic *UASp-venus::TTLL5* fly strain. *ApplGal4* and *UAS-*
544 *mito::GFP* were kindly provided by Simon Bullock's group (Vagnoni et al., 2016).

545 **Western blotting**

546 Western blotting performed with ovarian extracts was carried out with 10-20 pairs of ovaries
547 for each genotype. Newly hatched females of the indicated genotypes were collected and
548 crossed with *w* males in fresh vials with ample yeast food for two to three days. Fully
549 developed ovaries were then dissected and collected. The samples were directly lysed in
550 Laemmli buffer, boiled at 95°C for 10 min, and analyzed by SDS-PAGE. The following
551 primary antibodies were used: mouse 1D5 (1:500, Synaptic System), mouse GT335 (1:200,
552 Adipogen), mouse DM1A (1:1,000, Sigma), mouse tyrosinated α-tubulin (1:1,000, Sigma),
553 rabbit GFP (1:2,000, Sigma), rabbit GAPDH (1:1,000, GeneTex), rabbit TTLL5 (1:500,
554 GenScript), mouse BicD (1B11 plus 4C2, 1:5) (Suter and Steward, 1991), rabbit KHC
555 (1:1,000, cytoskeleton). Secondary antibodies were HRP-linked goat anti-mouse (1:1,0000,
556 GE Healthcare) and HRP-linked goat anti-rabbit (1:10,000, GE Healthcare). Antibodies were
557 incubated in 5% non-fat milk PBST (PBS with 0.1 % Triton X-100) and washed with PBST.
558 Chemiluminescence detection was done with the Amersham imager 600 (GE Healthcare).

559 **Mass Spectrometry**

560 Proteins were extracted from the ovaries of 100 3-day-old, well-fed females of each
561 genotype, crossed to wild-type males, and proteins were boiled and run on SDS-PAGE. The
562 gel was then stained with Coomassie Blue. The gel pieces containing the α-tubulin region
563 were cut, alkylated, and digested by trypsin N (ProtiFi) for 3 hours at 55°C. C-terminal
564 peptides of α-tubulin were analyzed by liquid chromatography (LC)-MS/MS (PROXEON
565 coupled to a QExactive mass spectrometer, Thermo Fisher Scientific). Samples were
566 searched against the UniProtKB *Drosophila* database using Pipeline, PEAKS, Easyprot and
567 MSfragger as search engines. Peptides were shown by PSM value (peptide spectrum
568 match). To avoid repetition of total PSM quantification, we searched only for one type of
569 PTM in an analysis per time. Total PSM indicates the sum of PSMs of primary C-terminal
570 peptides with either glutamylation or glycylation modifications or non-modified peptides.

571 **Ooplasmic streaming in living oocytes**

572 Three days old females were kept together with wild-type males under non-crowding
573 conditions at 25°C on food containing dry yeast. The determination of ooplasmic streaming

574 was based on the method of Lu and colleagues (Lu et al., 2016). Ovaries were directly
575 dissected in 10 S halocarbon oil (VWR), and egg chambers were teased apart in the oil drop
576 on 24×50 mm coverslips (VWR). Living Stage 10B oocytes were directly observed and
577 imaged under the 60×1.4 NA oil immersion objective on a Nikon W1 LIPSI spinning disk with
578 a 2x Photometrics Prime BSI CMOS camera. Time-lapse images were acquired every 2s for
579 2 min under bright-field (BF) controlled by Nikon Elements software. Flow tracks were
580 generated by kymographs using Fiji (Schindelin et al., 2012) plugin Multi Kymograph
581 (HTTPS:// imagej.net/ Multi _Kymograph).

582 **Immunostaining and confocal microscopy**

583 Ovaries were dissected in 1× PBS and fixed in buffer (200 µl 4% formaldehyde (Sigma), 600
584 ul Heptane (Merck Millipore), 20 ul DMSO (Sigma) for each group) for 20 min. Ovaries were
585 then blocked in 2% milk powder in PBST (PBS, 0.5% Triton X-100). Samples were
586 incubated with rabbit anti-Staufen (1:2,000) (St Johnston et al., 1991), mouse anti-BicD
587 (1B11 plus 4C2, 1:5) (Suter and Steward, 1991), rabbit anti-Khc (1:150, Cytoskeleton), rabbit
588 anti-GFP (1:200, Sigma) and mouse anti-1D5 (1:150, Synaptic System) at 4°C overnight,
589 and incubated with secondary Alexa Fluor goat anti-mouse Cy3 (1:400, Jackson
590 ImmonoResearch) and Alexa Fluor goat anti-rabbit 488 (1:400, Life technologies Thermo
591 Fischer) at room temperature for 3h. DNA and nuclei were stained using Hoechst 33528
592 (Thermo Fischer Scientific) for 10 min. Mounted samples were imaged with a Leica TCS
593 SP8 confocal microscope equipped with a 63×1.40 oil lens and controlled by the Las X
594 software (Leica). Images of single focal planes and 12 µm Z projection were acquired. The
595 crescent length of Staufen was processed by the Fuji segmented line tool based on a single
596 plane. The data were shown as means ± SEM by Prism 5 (GraphPad software). The
597 statistical significance was determined by an unpaired two-tailed non-parametric t-test
598 (Mann-Whitney test). For the Khc intensity analysis, the intensity of fluorescence in the
599 oocyte was plotted and the intensity charts were generated using Fiji's “Analyze-Plot profile”
600 function.

601 **Mitochondrial transport in *Drosophila* wing neurons**

602 Mitochondrial transport in *Drosophila* wing neurons was tracked as described (Vagnoni and
603 Bullock, 2016). In brief, 1-2 days old flies were anesthetized with CO_2 and immobilized in a
604 custom-built chamber formed of two No.1.5 24×50 mm coverslips (VWR). Imaging of wings
605 was performed with a Nikon W1 LIPSI spinning disk microscope equipped with a 2x
606 Photometrics Prime BSI CMOS camera and a 60×1.4 NA oil immersion lens. Time-lapse

607 video of a single focal plane was acquired with an acquisition rate of 0.5 frame/s for 3 min for
608 Mito::GFP using a 488 nm laser.

609 Quantification of the movements was performed in Fiji. At least 7 wings of each genotype
610 were tracked for quantification. A region of the wing arch of the L1 vein was selected and
611 straightened with the Straighten plugin (Eva Kocsis, NIH, MD). For each "run", the total
612 trafficking distance of more than 2 µm was defined as "motile mitochondria". To exclude the
613 oscillatory movements of mitochondria, a minimal instant velocity between each frame was
614 defined at 0.2 µm/s. Transported mitochondria were manually tracked by the manual
615 tracking plugin (Fabrice Cordelières, Institute Curie, France). Kymographs of individual
616 mitochondria were produced using the Fiji (Schindelin et al., 2012) plugin Multi Kymograph
617 (HTTPS:// imagej.net/ Multi _Kymograph). Run length, instant velocity values, and total
618 running, trafficking & pausing times were exported into Excel for analysis. The data are
619 shown as means ± SEM by Prism 5 (GraphPad). The statistical significance was determined
620 with the student's t-test.

621 **Sequence alignment**

622 Sequences were aligned by CLC Sequence Viewer 8.0 software (Qiagen). The UniProtKB
623 accession numbers are as follows: *HsTTL*: Q8NG68; *HsTTLL5*: Q6EMB2; *MmTTLL5*:
624 Q8CHB8; *DmTTLL5*: Q9VBX5;

625 **Acknowledgments**

626 We thank Simon L. Bullock (Cambridge, UK) for *ApplGal4* and *UAS-mito::GFP* fly lines,
627 Michel Steinmetz (Paul Scherrer Institute, Switzerland), and the Carsten Janke (Institute
628 Curie, France) laboratory members for discussions and suggestions. We also thank the
629 University of Bern (Switzerland) Mass Spectrometry center members Sophie Braga Lagache
630 and Natasha Buchs for performing the MS experiments and Manfred Heller and Anne-
631 Christine Uldry for peptide analysis and discussion of the results.

632

633 **Support**

634 This work was financially supported by the project grants 31003A_173188 and
635 310030_205075 from the Swiss National Science Foundation (SNF; https://www.snf.ch/en)
636 to BS. Equipment support was by an equipment grant from SNF (316030_150824) to BS
637 and by the University of Bern (https://www.unibe.ch). Additional salary and material support

638 were received from the University of Bern (https://www.unibe.ch) to BS. The funders had no
639 role in the study design, data collection, analysis, decision to publish, or manuscript
640 preparation.

641 The authors declare no competing financial interests.

642 Author contributions: Mengjing Bao, Beat Suter, and Maria Paula Vazquez-Pianzola
643 conceived the project and designed the experiments. Mengjing Bao, Beat Suter, Ruth Dörig,
644 and Dirk Beuchle performed the experiments and analyzed the data; Mengjing Bao and Beat
645 Suter wrote the manuscript.

646

647 **Reference**

648 Arce, C.A., J.A. Rodriguez, H.S. Barra, and R. Caputo. 1975. Incorporation of L-tyrosine, L-
649 phenylalanine, and L-3,4-dihydroxyphenylalanine as single units into rat brain tubulin.
650 *Eur J Biochem*. 59:145-149.
651 Bodakuntla, S., X. Yuan, M. Genova, S. Gadadhar, S. Leboucher, M.C. Birling, D. Klein, R.
652 Martini, C. Janke, and M.M. Magiera. 2021. Distinct roles of α- and β-tubulin
653 polyglutamylation in controlling axonal transport and in neurodegeneration. *EMBO J*.
654 40:e108498.
655 Bré, M.H., V. Redeker, M. Quibell, J. Darmanaden-Delorme, C. Bressac, J. Cosson, P.
656 Huitorel, J.M. Schmitter, J. Rossler, T. Johnson, A. Adoutte, and N. Levilliers. 1996.
657 Axonemal tubulin polyglycylation probed with two monoclonal antibodies: widespread
658 evolutionary distribution, appearance during spermatozoan maturation and possible
659 function in motility. *J Cell Sci*. 109 (Pt 4):727-738.
660 Brendza, R.P., L.R. Serbus, J.B. Duffy, and W.M. Saxton. 2000. A function for kinesin I in
661 the posterior transport of oskar mRNA and Staufen protein. *Science*. 289:2120-2122.
662 Claussen, M., and B. Suter. 2005. BicD-dependent localization processes: from Drosophila
663 development to human cell biology. *Ann Anat*. 187:539-553.
664 Devambez, I., J. van Dijk, S. Benlefki, S. Layalle, Y. Grau, K. Rogowski, M.L. Parmentier,
665 and L. Soustelle. 2017. Identification of DmTTLL5 as a Major Tubulin Glutamylase in
666 the Drosophila Nervous System. *Sci Rep*. 7:16254.
667 Eddé, B., J. Rossier, J.P. Le Caer, E. Desbruyères, F. Gros, and P. Denoulet. 1990.
668 Posttranslational glutamylation of alpha-tubulin. *Science*. 247:83-85.
669 Gadadhar, S., G. Alvarez Viar, J.N. Hansen, A. Gong, A. Kostarev, C. Ialy-Radio, S.
670 Leboucher, M. Whitfield, A. Ziyyat, A. Touré, L. Alvarez, G. Pigino, and C. Janke.
671 2021. Tubulin glycylation controls axonemal dynein activity, flagellar beat, and male
672 fertility. *Science*. 371.
673 Gadadhar, S., S. Bodakuntla, K. Natarajan, and C. Janke. 2017. The tubulin code at a
674 glance. *J Cell Sci*. 130:1347-1353.
675 Hallak, M.E., J.A. Rodriguez, H.S. Barra, and R. Caputto. 1977. Release of tyrosine from
676 tyrosinated tubulin. Some common factors that affect this process and the assembly
677 of tubulin. *FEBS Lett*. 73:147-150.
678 Hollenbeck, P.J., and W.M. Saxton. 2005. The axonal transport of mitochondria. *J Cell Sci*.
679 118:5411-5419.
680 Janke, C., K. Rogowski, D. Wloga, C. Regnard, A.V. Kajava, J.M. Strub, N. Temurak, J. van
681 Dijk, D. Boucher, A. van Dorsselaer, S. Suryavanshi, J. Gaertig, and B. Eddé. 2005.

682 Tubulin polyglutamylase enzymes are members of the TTL domain protein family.
683 *Science*. 308:1758-1762.
684 Kalfayan, L., and P.C. Wensink. 1982. Developmental regulation of Drosophila alpha-tubulin
685 genes. *Cell*. 29:91-98.
686 Kato, Y., and A. Nakamura. 2012. Roles of cytoplasmic RNP granules in intracellular RNA
687 localization and translational control in the Drosophila oocyte. *Dev Growth Differ*.
688 54:19-31.
689 L'Hernault, S.W., and J.L. Rosenbaum. 1985. Chlamydomonas alpha-tubulin is
690 posttranslationally modified by acetylation on the epsilon-amino group of a lysine.
691 *Biochemistry*. 24:473-478.
692 Lee, G.S., Y. He, E.J. Dougherty, M. Jimenez-Movilla, M. Avella, S. Grullon, D.S. Sharlin, C.
693 Guo, J.A. Blackford, Jr., S. Awasthi, Z. Zhang, S.P. Armstrong, E.C. London, W.
694 Chen, J. Dean, and S.S. Simons, Jr. 2013. Disruption of Ttll5/stamp gene (tubulin
695 tyrosine ligase-like protein 5/SRC-1 and TIF2-associated modulatory protein gene) in
696 male mice causes sperm malformation and infertility. *J Biol Chem*. 288:15167-15180.
697 Lu, W., M. Lakonishok, A.S. Serpinskaya, D. Kirchenbüechler, S.C. Ling, and V.I. Gelfand.
698 2018. Ooplasmic flow cooperates with transport and anchorage in. *J Cell Biol*.
699 217:3497-3511.
700 Lu, W., M. Winding, M. Lakonishok, J. Wildonger, and V.I. Gelfand. 2016. Microtubule-
701 microtubule sliding by kinesin-1 is essential for normal cytoplasmic streaming in
702 Drosophila oocytes. *Proc Natl Acad Sci U S A*. 113:E4995-5004.
703 Magiera, M.M., and C. Janke. 2014. Post-translational modifications of tubulin. *Curr Biol*.
704 24:R351-354.
705 Mahalingan, K.K., E. Keith Keenan, M. Strickland, Y. Li, Y. Liu, H.L. Ball, M.E. Tanner, N.
706 Tjandra, and A. Roll-Mecak. 2020. Structural basis for polyglutamate chain initiation
707 and elongation by TTLL family enzymes. *Nat Struct Mol Biol*. 27:802-813.
708 McKenney, R.J., W. Huynh, R.D. Vale, and M. Sirajuddin. 2016. Tyrosination of α-tubulin
709 controls the initiation of processive dynein-dynactin motility. *Embo j*. 35:1175-1185.
710 Monteith, C.E., M.E. Brunner, I. Djagaeva, A.M. Bielecki, J.M. Deutsch, and W.M. Saxton.
711 2016. A Mechanism for Cytoplasmic Streaming: Kinesin-Driven Alignment of
712 Microtubules and Fast Fluid Flows. *Biophys J*. 110:2053-2065.
713 Natarajan, K., S. Gadadhar, J. Souphron, M.M. Magiera, and C. Janke. 2017. Molecular
714 interactions between tubulin tails and glutamylases reveal determinants of
715 glutamylation patterns. *EMBO Rep*. 18:1013-1026.
716 Pilling, A.D., D. Horiuchi, C.M. Lively, and W.M. Saxton. 2006. Kinesin-1 and dynein are the
717 primary motors for fast transport of mitochondria in Drosophila motor axons. *Mol Biol*
718 *Cell*. 17:2057-2068.
719 Port, F., H.M. Chen, T. Lee, and S.L. Bullock. 2014. Optimized CRISPR/Cas tools for
720 efficient germline and somatic genome engineering in Drosophila. *Proc Natl Acad Sci*
721 *U S A*. 111:E2967-2976.
722 Preston, S.F., G.G. Deanin, R.K. Hanson, and M.W. Gordon. 1979. The phylogenetic
723 distribution of tubulin:tyrosine ligase. *J Mol Evol*. 13:233-244.
724 Prota, A.E., M.M. Magiera, M. Kuijpers, K. Bargsten, D. Frey, M. Wieser, R. Jaussi, C.C.
725 Hoogenraad, R.A. Kammerer, C. Janke, and M.O. Steinmetz. 2013. Structural basis
726 of tubulin tyrosination by tubulin tyrosine ligase. *J Cell Biol*. 200:259-270.
727 Redeker, V., N. Levilliers, J.M. Schmitter, J.P. Le Caer, J. Rossier, A. Adoutte, and M.H. Bré.
728 1994. Polyglycylation of tubulin: a post-translational modification in axonemal
729 microtubules. *Science*. 266:1688-1691.
730 Redeker, V., N. Levilliers, E. Vinolo, J. Rossier, D. Jaillard, D. Burnette, J. Gaertig, and M.H.
731 Bré. 2005. Mutations of tubulin glycylation sites reveal cross-talk between the C
732 termini of alpha- and beta-tubulin and affect the ciliary matrix in Tetrahymena. *J Biol*
733 *Chem*. 280:596-606.
734 Redeker, V., R. Melki, D. Promé, J.P. Le Caer, and J. Rossier. 1992. Structure of tubulin C-
735 terminal domain obtained by subtilisin treatment. The major alpha and beta tubulin
736 isotypes from pig brain are glutamylated. *FEBS Lett*. 313:185-192.

737 Rogowski, K., F. Juge, J. van Dijk, D. Wloga, J.M. Strub, N. Levilliers, D. Thomas, M.H. Bré,
738 A. Van Dorsselaer, J. Gaertig, and C. Janke. 2009. Evolutionary divergence of
739 enzymatic mechanisms for post-translational polyglycylation. *Cell*. 137:1076-1087.
740 Rogowski, K., J. van Dijk, M.M. Magiera, C. Bosc, J.C. Deloulme, A. Bosson, L. Peris, N.D.
741 Gold, B. Lacroix, M. Bosch Grau, N. Bec, C. Larroque, S. Desagher, M. Holzer, A.
742 Andrieux, M.J. Moutin, and C. Janke. 2010. A family of protein-deglutamylating
743 enzymes associated with neurodegeneration. *Cell*. 143:564-578.
744 Rüdiger, A.H., M. Rüdiger, J. Wehland, and K. Weber. 1999. Monoclonal antibody ID5:
745 epitope characterization and minimal requirements for the recognition of
746 polyglutamylated alpha- and beta-tubulin. *Eur J Cell Biol*. 78:15-20.
747 Schindelin, J., I. Arganda-Carreras, E. Frise, V. Kaynig, M. Longair, T. Pietzsch, S.
748 Preibisch, C. Rueden, S. Saalfeld, B. Schmid, J.Y. Tinevez, D.J. White, V.
749 Hartenstein, K. Eliceiri, P. Tomancak, and A. Cardona. 2012. Fiji: an open-source
750 platform for biological-image analysis. *Nat Methods*. 9:676-682.
751 Serbus, L.R., B.J. Cha, W.E. Theurkauf, and W.M. Saxton. 2005. Dynein and the actin
752 cytoskeleton control kinesin-driven cytoplasmic streaming in Drosophila oocytes.
753 *Development*. 132:3743-3752.
754 Sirajuddin, M., L.M. Rice, and R.D. Vale. 2014. Regulation of microtubule motors by tubulin
755 isotypes and post-translational modifications. *Nat Cell Biol*. 16:335-344.
756 St Johnston, D., D. Beuchle, and C. Nüsslein-Volhard. 1991. Staufen, a gene required to
757 localize maternal RNAs in the Drosophila egg. *Cell*. 66:51-63.
758 Suter, B. 2018. RNA localization and transport. *Biochim Biophys Acta Gene Regul Mech*.
759 1861:938-951.
760 Suter, B., and R. Steward. 1991. Requirement for phosphorylation and localization of the
761 Bicaudal-D protein in Drosophila oocyte differentiation. *Cell*. 67:917-926.
762 Szczesna, E., E.A. Zehr, S.W. Cummings, A. Szyk, K.K. Mahalingan, Y. Li, and A. Roll-
763 Mecak. 2022. Combinatorial and antagonistic effects of tubulin glutamylation and
764 glycylation on katanin microtubule severing. *Dev Cell*. 57:2497-2513.e2496.
765 Theurkauf, W.E., H. Baum, J. Bo, and P.C. Wensink. 1986. Tissue-specific and constitutive
766 alpha-tubulin genes of Drosophila melanogaster code for structurally distinct proteins.
767 *Proc Natl Acad Sci U S A*. 83:8477-8481.
768 Vagnoni, A., and S.L. Bullock. 2016. A simple method for imaging axonal transport in aging
769 neurons using the adult Drosophila wing. *Nat Protoc*. 11:1711-1723.
770 van Dijk, J., K. Rogowski, J. Miro, B. Lacroix, B. Eddé, and C. Janke. 2007. A targeted
771 multienzyme mechanism for selective microtubule polyglutamylation. *Mol Cell*.
772 26:437-448.
773 Wang, X., and T.L. Schwarz. 2009. The mechanism of Ca2+ -dependent regulation of
774 kinesin-mediated mitochondrial motility. *Cell*. 136:163-174.
775 Wang, X., D. Winter, G. Ashrafi, J. Schlehe, Y.L. Wong, D. Selkoe, S. Rice, J. Steen, M.J.
776 LaVoie, and T.L. Schwarz. 2011. PINK1 and Parkin target Miro for phosphorylation
777 and degradation to arrest mitochondrial motility. *Cell*. 147:893-906.
778 Weil, T.T. 2014. mRNA localization in the Drosophila germline. *RNA Biol*. 11:1010-1018.
779 Wloga, D., D.M. Webster, K. Rogowski, M.H. Bré, N. Levilliers, M. Jerka-Dziadosz, C. Janke,
780 S.T. Dougan, and J. Gaertig. 2009. TTLL3 Is a tubulin glycine ligase that regulates
781 the assembly of cilia. *Dev Cell*. 16:867-876.
782 Wolff, A., B. de Néchaud, D. Chillet, H. Mazarguil, E. Desbruyères, S. Audebert, B. Eddé, F.
783 Gros, and P. Denoulet. 1992. Distribution of glutamylated alpha and beta-tubulin in
784 mouse tissues using a specific monoclonal antibody, GT335. *Eur J Cell Biol*. 59:425-
785 432.
786 Zimyanin, V.L., K. Belaya, J. Pecreaux, M.J. Gilchrist, A. Clark, I. Davis, and D. St Johnston.
787 2008. In vivo imaging of oskar mRNA transport reveals the mechanism of posterior
788 localization. *Cell*. 134:843-853.

789

790 **Table 1) Conservation between mammalian *TTLL5 and Drosophila TTLL5***

791 Residues labeled in red are critical residues for α-tubulin glutamylation by murine TTLL5 and are
792 conserved in human and *Drosophila* TTLL5 (van Dijk et al., 2007, Natarajan et al., 2017).

	K131 β6-7 loop (R188) R225 E366 N368
Mm TTLL5	TRKDR—KPVASSRGRG[1)]VY---VRLYVL---LLEVNLSP
Hs TTLL5	TRKDR—KPVASSRGRG VY---VRLYVL---LLEVNLSP
	K282 β6-7 loop (R339) R376 E517 N519
Dm TTLL5	TRKDR--KPAASSRGRG I F---LRVYVL---LLEI NLSP

793 [1)] The critical domain of the β6-7 loop is highlighted with a yellow background.

794

795 **Table 2) Role of *TTLL5* for the glutamylation of the C-terminal domain of αTub84B/D.**
796 Frequency of glutamylated C-terminal peptides (containing the entire primary sequence) in *w* controls,
797 *TTLL5*^{pBac,} and *TTLL5*^{MiEx} mutants containing modifications of 1E, 2E, or 3Es.

	w[1)]	*TTLL5*^{pBac} (*%E mod*)	*TTLL5*^{MiEx}
+1	41	0	0
+2	14	0	0
+3	7	0	0
Total Glu modifications[2)]	62	0	0

798 [1)] The total peptide numbers (n) were indicated by the values of total PSM (peptide spectrum match) of the full
799 primary C-terminal αTub84B/D sequence. The n for *w*, *TTLL5*^{pBac}, and *TTLL5*^{MiEx} were 56, 29, and 7,
800 respectively.
801 [2)] Total Glu modifications show the sum of the three frequencies. The ratio was quantified based on the
802 glutamylated C-terminal αTub84B/D PSM values divided by total PSM.

803

804 **Table 3) Conservation between *TTL* and *TTLL5***

805 Many critical residues of human TTL (red) are conserved in *Drosophila,* mouse, and human TTLL5
806 (Prota et al., 2013).

	R202 R222 D318 E331 N333 P336
Hs TTL	IRSW—VLRTA-----FDFM—LI EVNGAPA
	R376 R398 D504 E517 N519 P522
Dm TTLL5	LRVY---I VRLA-----FDIL----LLEI NL SPS
	R225 R247 D353 E366 N368 P371
Mm TTLL5	VRLY---LARFA-----FDVL---LLEVNL SPS
	R225 R247 D353 E366 N368 P371
Hs TTLL5	VRLY---LARFA-----FDVL---LLEVNL SPS

807

808

809 **Figure legends**

810 **Fig. 1 Mass spectrometry analysis of glutamylation of the C-terminal domains of**
811 ***Drosophila* α-tubulins.** A) Schematic representation showing how the C-terminal regions of
812 αTub84B/D can be modified by glutamic acid residues added to the side chains of E443,
813 E445, E448, and E449 in *Drosophila* ovaries. B) The C-terminal peptides containing the
814 complete primary sequence were analyzed. The structure of the different C-terminal tail
815 peptides of αTub84B/D modified by glutamylation is shown starting with G442. Different
816 combinations of Glu side chain modifications were found added at positions E443, E445,
817 E448, and E449 of αTub84B/D. Schemes were drawn by biorender.com.

818 **Fig. 2 Schematic representation of the *Drosophila TTLL5* gene, TTLL5, TTLL5^{MiEx}, and**
819 **Venus::TTLL5 proteins.** A) The *TTLL5* gene structure is based on the Flybase data for the
820 CG31108-RA transcript. The positions of the loss-of-function mutations are marked on the
821 *TTLL5* gene. Grey triangles: transposon insertions. Grey asterisks: codons targeted for
822 generating InDels and point mutations. All *TTLL5* alleles were analyzed as hemizygous
823 animals over *Df(3R)BSC679*, which removes the region of the *TTLL5* gene. B) Western blot
824 from the soluble fraction of ovarian extracts. *w* (*TTLL5*$^{+}$/$^{+}$*),* which contains two wild-type
825 copies of *TTLL5*, expressed the highest levels of TTLL5. The TTLL5 signal is strongly
826 reduced or abolished in the null mutants *TTLL5*^{pBac}/$^{-}$*, TTLL5*^{Mi}/$^{-}$, and *TTLL5*^{MiEx}/$^{-}$ compared to
827 *w.* The hemizygous *TTLL5*$^{+}$ ovaries (*TTLL5*$^{+}$/$^{-}$) expressed less TTLL5 than *w.* The signal of
828 an unspecific band (labeled with *), produced after a short exposure, was used as the
829 loading control. In the following, we will refer to the genotypes as *w* for the control (*TTLL5*$^{+}$/$^{+}$)
830 and *TTLL5*^{allele} for the hemizygous mutants *(TTLL5*^{allele}/$^{-}$).

831 **Fig. 3 *TTLL5* is required for the glutamylation of α-tubulin in ovaries.** A), C) Sites on
832 αTub84B/D, expected to be recognized by the antibody against monoglutamylation (A),
833 GT335, and by the 1D5 antibody (C, recognizing polyglutamylation), respectively. B), D) The
834 glutamylation signal, produced by western blotting with the GT335 and 1D5 antibodies,
835 respectively, is lower in *TTLL5*^{pBac}*, TTLL5*^{Mi}, and *TTLL5*^{MiEx} than in the *w* control but is
836 restored and even elevated in mutant ovaries that were rescued by
837 *MattubGal4>Venus::TTLL5*. The up-shifted bands recognized by 1D5 can be seen in the
838 rescued *TTLL5*^{pBac} and *TTLL5*^{Mi} mutants. The total tyrosinated α-tubulin levels seemed
839 unaffected by the TTLL5 levels. α-tubulin and GAPDH served as loading controls. E) The
840 genotypes and rationale of the *TTLL5* alleles generated by CRISPR/Cas9 are listed. The
841 selected residues are predicted to be either important for the glutamylation or tyrosination
842 function based on the alignment shown in **Tables 3** and **4**. F) Western blotting shows that

843 the polyglutamylation signal is absent in all point mutants. *w* with two copies of *TTLL5*$^{+}$ is the
844 wild-type control and the hemizygous *TTLL5*$^{TRK282>KGK282}$ still contains the crucial K282
845 residue and behaves like the control. 1D5 signals relative to the loading controls decrease
846 slightly in the hemizygous situation with only one *TTLL5*$^{+}$ copy. G) Stronger up-shifted bands
847 were observed with the polyglutamylation antibody (1D5) upon *Venus::TTLL5*
848 overexpression in wild-type ovaries. Total α-tubulin levels were similar in samples with
849 excessive expression of *TTLL5.* GAPDH was a loading control. All mutant *TTLL5* alleles
850 were analyzed as hemizygous animals over *Df(3R)BSC679*. The genotypes for rescues
851 were *MattubGal4>UAS-Venus::TTLL5;TTLL5*^{alleles}*/Df(3R)BSC679.* The genotypes for
852 *Venus::TTLL5* overexpression were *MattubGal4>UAS-Venus::TTLL5.*

853 **Fig. 4 Spatial distribution of polyglutamylated microtubules in the oocyte.** Confocal
854 micrographs showing representative oocytes and follicle cells from early to late stages of *w*
855 controls and *TTLL5*^{MiEx} mutants. Polyglutamylation (1D5) signals are shown in magenta and
856 Hochest in blue. A signal is seen in follicle cells and oocytes from previtellogenic to late-
857 stage oocytes. For the S10B oocytes, a high-power magnification for the posterior half is
858 shown, too. At this stage, a slightly biased 1D5 signal intensity was seen in the cortical
859 region of the oocyte. The 1D5 signal is virtually absent in the *TTLL5* mutants. Imaging
860 conditions and confocal microscope settings were identical for the two genotypes. The
861 genotype of the control was *w.* Genotypes for *TTLL5*^{MiEx} were *TTLL5*^{MiEx}*/Df(3R)BSC679*.

862 **Fig. 5 Effect of *TTLL5* on Staufen localization refinement in oocytes.** A)-D) Confocal
863 micrographs showing S10B oocytes of *w* controls and *TTLL5*^{pBac}*, TTLL5*^{Mi}, and *TTLL5*^{MiEx}
864 mutants (A, B), *TTLL5*^{pBac}*, TTLL5*^{Mi}, and *TTLL5*^{MiEx} mutants rescued by *Mattub4>UASP-*
865 *Venus::TTLL5* (C), and *w* controls, *TTLL5*^{E517A}*, TTLL5*^{P522A}*,* and *TTLL5*^{R339A} mutants (D). Anti-
866 Staufen is shown in green, anti-GFP in red, and Hoechst in blue. E) Quantification of the
867 Staufen crescent length along the posterior cortex based on A-D) *** $p<0.005$. z stack:
868 12µm. F) Confocal micrographs showing previtellogenic and S9 egg chambers of *w*
869 controls, *TTLL5*^{pBac}*, TTLL5*^{MiEx}*,* and *TTLL5*^{E517A} mutants. Staufen signal is shown in green,
870 and Hoechst in blue. Scale Bar: 25µm. *TTLL5*^{MiEx} and *TTLL5*^{E517A} were hemizygous over
871 *Df(3R)BSC679*. The genotype for *TTLL5*^{pBac} was *MattubGal4/+; TTLL5*^{pBac}*/Df(3R)BSC679.*
872 The genotypes of the rescued animals were *MattubGal4/UAS-Venus::TTLL5; TTLL5*
873 ^{alleles}*/Df(3R)BSC679.*

874 **Fig. 6 Role of *TTLL5* in fast ooplasmic streaming.** A) Example of an S10B oocyte used
875 for particle flow measurements based on time-lapse movies of ooplasmic streaming
876 (Mov.S1-S5). Scale Bar: 25 µm. B) Representative kymographs of particles in oocytes of *w*

877 controls, *TTLL5*^{MiEx} mutants, *TTLL5*^{E517A} mutants, and *TTLL5*^{MiEx} mutants rescued by
878 overexpression of the *UASP-Venus::TTLL5* transgene. *UASP-Venus::TTLL5* overexpression
879 in the wild-type background is also shown. Kymographs were generated along a line close to
880 the cortex on one side of the ooplasm (region marked by a yellow line in A). 2 min time-lapse
881 movies were taken. For the mutants, two Kymographs are shown from two different flies
882 each. 100% of the S10B control oocytes analyzed (n=17) showed circular unidirectional
883 streaming. On the contrary, 76% *TTLL5*^{MiEx} oocytes showed an abnormal streaming pattern
884 (n=21). 100% of *TTLL5*^{E517A} oocytes showed an abnormal streaming pattern (n=10). 71 % of
885 the rescued oocytes showed circular unidirectional streaming (n=7). The genotype of the
886 control was *w* or *+/Df(3R)BSC679.* Genotypes for *TTLL5*^{MiEx} and *TTLL5*^{E517A} were both over
887 *Df(3R)BSC679*. The genotype of the rescued flies was *MattubGal4/UAS-Venus::TTLL5;*
888 *TTLL5*^{MiEx}*/Df(3R)BSC679.* The genotype of *TTLL5* overexpression (5 oocytes) was
889 *MattubGal4/UAS-Venus::TTLL5.* C) Schematic representation of different streaming patterns
890 observed. When *TTLL5* was sufficient, the particles showed a unidirectional streaming
891 pattern. When *TTLL5* is insufficient or inactive, the direction of streaming was disordered, or
892 the streaming was partially disrupted.

893 **Fig. 7 Role of *TTLL5* for kinesin expression and distribution in ovaries** A), B) Khc levels
894 remained unchanged between *w* control, *TTLL5* deficient mutants, rescued *TTLL5* mutants,
895 and *TTLL5* overexpressing ovaries. Anti-GFP antibodies reveal the expression of
896 *Venus:TTLL5.* GAPDH served as the loading control. C) E) Confocal micrographs showing
897 the Khc distribution in stage 10B oocytes. C) White arrowheads point to the posterior
898 enrichment of Khc along the cortical region in the wild-type control and TTLL5
899 overexpressing oocytes. D) Blind quantification of the posterior enrichment of Khc. The
900 frequency of oocytes with posterior enrichment is shown graphically and numerically. n=
901 number of oocytes evaluated. E) A white line was drawn along the anterior-posterior axis of
902 the oocyte using Fiji. The lines start at the nurse cell oocyte border on the left and end at the
903 posterior follicle cells. The line width was 50 units. G) Intensity charts were plotted based on
904 the line drawn along the AP axis in E). The orange arrowheads in the oocytes and the
905 intensity charts point to the regions showing higher Khc accumulation in the inner region of
906 the oocyte. F) Fraction of the oocytes that showed inner hyperaccumulation of Khc were
907 quantified. n= number of oocytes evaluated. The percentage of oocytes showing inner
908 enrichment of Khc is shown graphically and numerically. Judging Khc distribution was done
909 blindly by two persons. The fractions were taken from the mean values obtained from the
910 two persons. Scale Bar: 25μm. The Khc signal is shown in green, and Hoechst in blue. The
911 genotype for controls was *w* or *+/Df(3R)BSC679.* Genotype for *TTLL5*^{pBac}: *MattubGal4/+,*

912 *TTLL5^{pBac}/Df(3R)BSC679*; *TTLL5^{MiEx}: TTLL5^{MiEx}/Df(3R)BSC679*. Genotype for *TTLL5*
913 overexpression: *MattubGal4/UAS-Venus::TTLL5.*

914 **Fig. 8 Role of *TTLL5* in the transport of mitochondria in the wing nerves.** A)
915 Representative still image of GFP-labelled mitochondria in axons of the L1 vein of both
916 control and *TTLL5^{E517A}* wings. The position of the L1 region is indicated in the picture above.
917 B) Scheme of the transport behavior of the mitochondria in the wing neuron. See the main
918 text for a detailed description. The schema was drawn by biorender.com. C-F) Mean values
919 of run length, net velocity, trafficking velocity, and pausing time ratio in the control and the
920 *TTLL5 ^{E517A}* mutant for both anterograde and retrograde transport. C) The run length is the
921 sum of the distances traveled by individual mitochondria in a trafficking state. D) The net
922 velocity indicates run distance divided by run time. The run time is the sum of the total
923 pausing time plus the total trafficking time. E) Trafficking velocity indicates the mean of the
924 instant velocity of the trafficking mitochondria. F) Pausing time ratio was calculated as total
925 pausing time divided by run time. Total pausing time was the sum of the time when the
926 mitochondria were pausing. G) Kymographs were generated from 3 representative
927 mitochondria in the control and the *TTLL5^{E517A}* mutant. Yellow arrowheads indicate the
928 pauses of selected mitochondria over the 3 min time window. H) The mean values of
929 pausing frequency. Pausing frequency indicates the number of pauses divided by run length.
930 Mitochondria were quantified from 7 control fly wings and 8 *TTLL5^{E517A}* fly wings. The
931 numbers of mitochondria (n) analyzed for the anterograde control, anterograde *TTLL5^{E517A}*,
932 retrograde control, and retrograde *TTLL5^{E517A}* were 46, 36, 25, and 21, respectively. ***
933 $p<0.005$, ** $p<0.01$. Genotypes for controls were a mixture of *ApplGal4;UAS-*
934 *Mito::GFP;+/Df(3R)BSC679* and *ApplGal4;UAS-Mito::GFP;TTLL5 ^{E517A}/+***.** Genotypes for
935 *TTLL5^{E517A}* mutants were *ApplGal4; UAS-Mito::GFP; TTLL5^{E517A}/Df(3R)BSC679***.**

Fig. 1

A **α-tubulin isotypes in *Drosophila* ovaries**

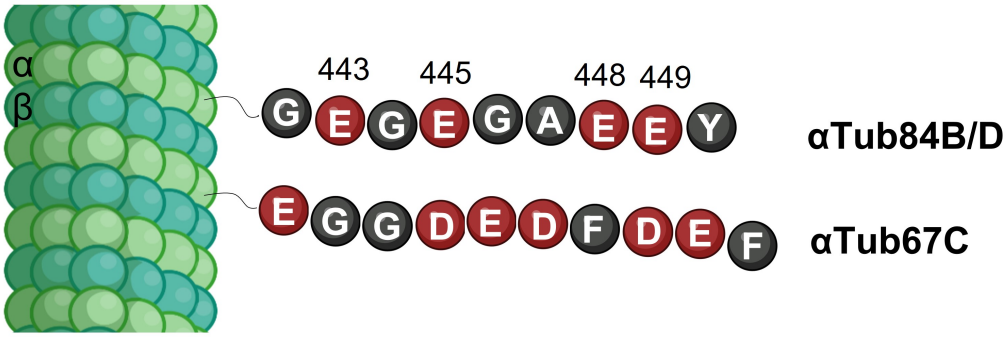

E-residues were found added at the αTub84B/D positions E443, E445, E448 and E449.

B **Glutamylation on E residues in the C-terminal domain of αTub84B/D**

GEGEGAEEY E	GEGEGAEEY E	GEGEGAEEY E	GEGEGAEEY E
GEGEGAEEY EE	GEGEGAEEY EE	GEGEGAEEY EE	GEGEGAEEY EE
GEGEGAEEY EEE	GEGEGAEEY EEE	GEGEGAEEY EEE	GEGEGAEEY EEE
GEGEGAEEY E E	GEGEGAEEY E EE	GEGEGAEEY E E	GEGEGAEEY E EE
GEGEGAEEY EEE	GEGEGAEEY E E E		

Fig. 2

A

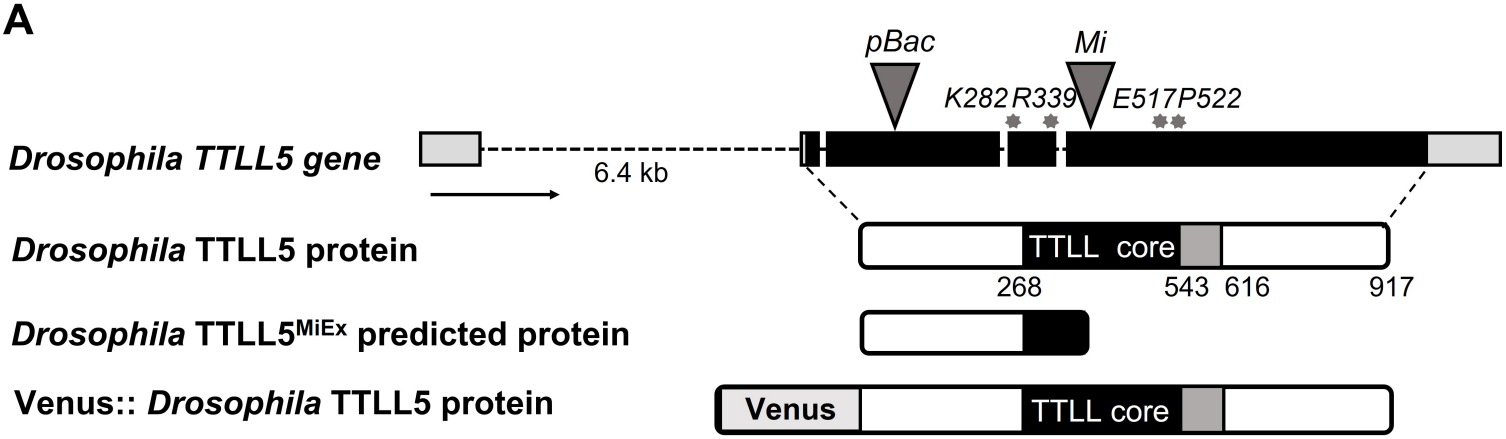
pBac
Mi
K282 R339
E517 P522
Drosophila TTLL5 gene
6.4 kb
Drosophila TTLL5 protein
TTLL core
268
543 616
917
Drosophila TTLL5MiEx predicted protein
Venus:: Drosophila TTLL5 protein
Venus
TTLL core

B

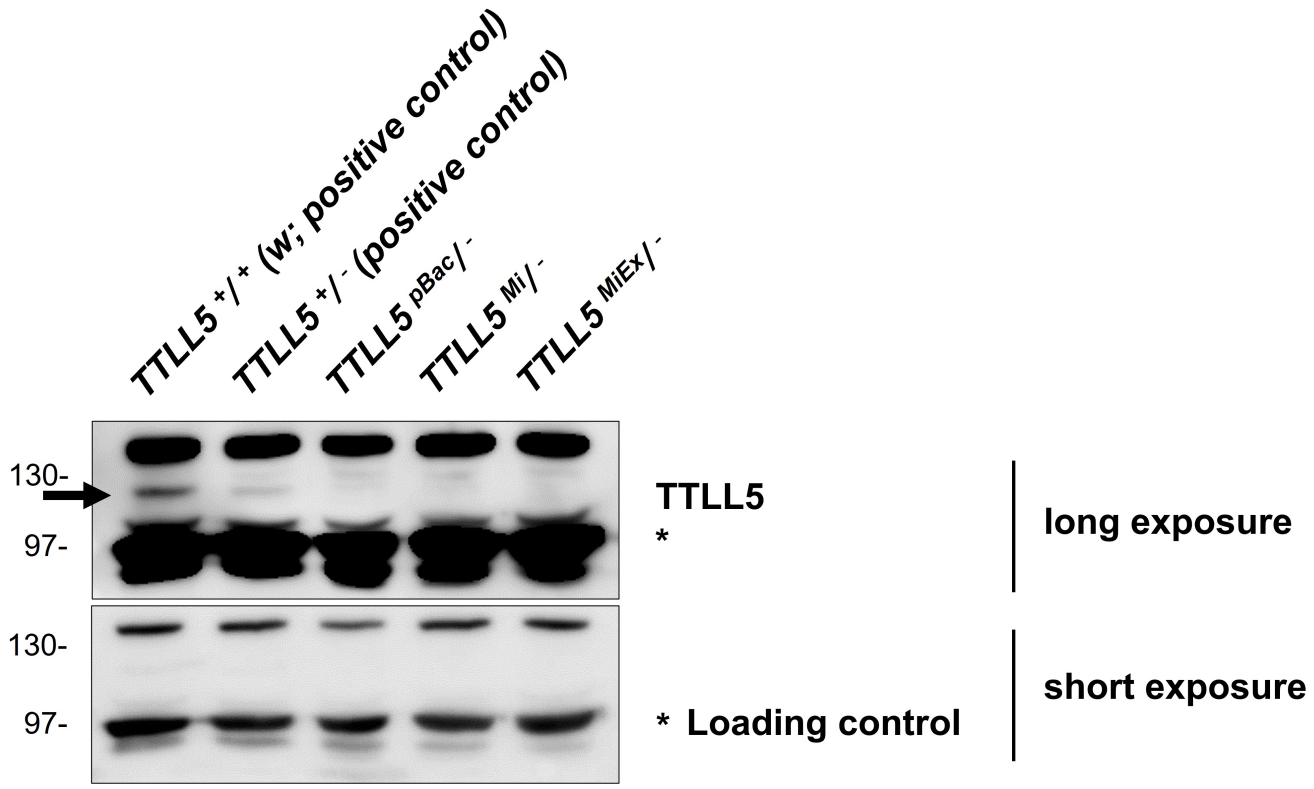
TTLL5 +/+ (w; positive control)
TTLL5 +/- (positive control)
TTLL5 pBac/-
TTLL5 Mi/-
TTLL5 MiEx/-
130-
97-
TTLL5
*
long exposure
130-
97-
* Loading control
short exposure

Fig. 3

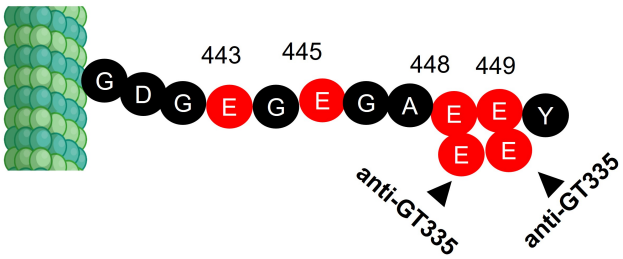

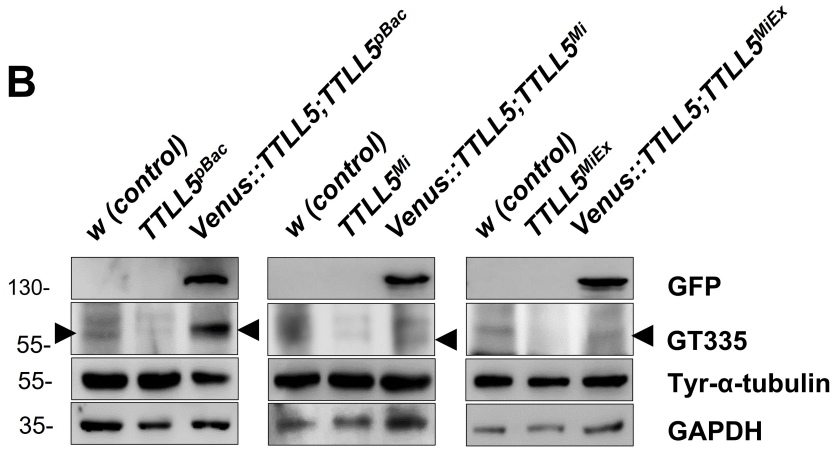

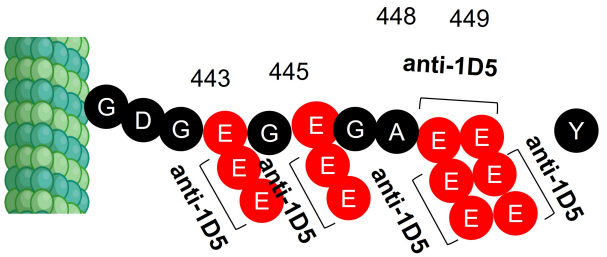

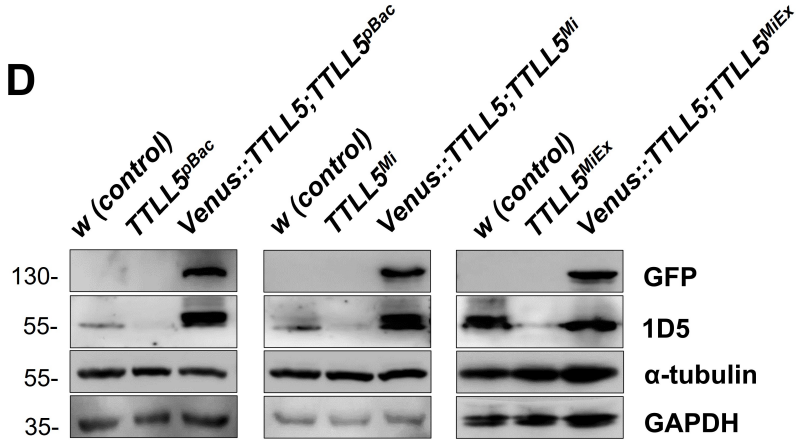

E

Residues of *Drosophila TTLL5*	Function	Corresponding residues in mammalian TTLL5 or TTL	Mutations
E517	ATP/ADP binding	E336 of MmTTLL5 E331 of HsTTL	*WLLE517>S* *E517A*
K282	ATP/ADP binding	K131 of MmTTLL5	*K282 stop codon* *TRK282D>N* *TRK282>KGK*
R339	(In β6-7 loop) stabilizes tubulin to the active site of TTLL5	R188 of MmTTLL5	*R339A*
P522	(Conserved residue of human TTL) anchors TTL to α-tubulin	P336 of HsTTL	*P522A*

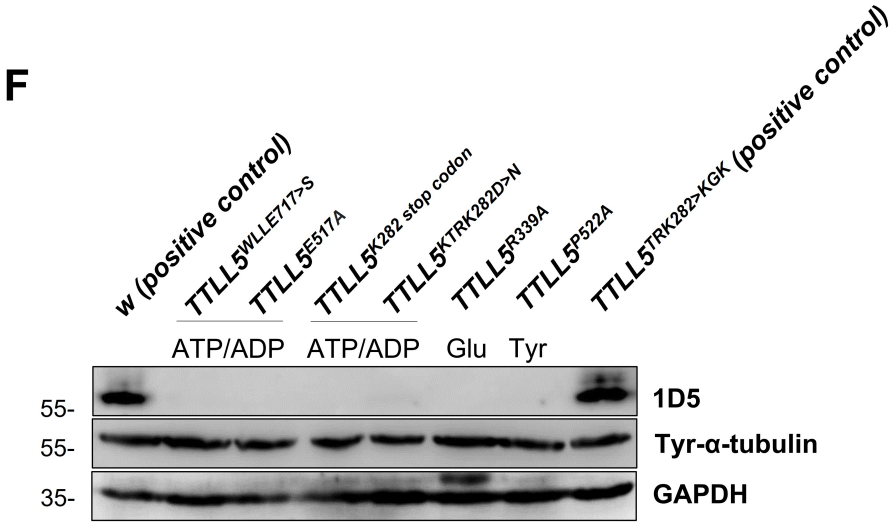

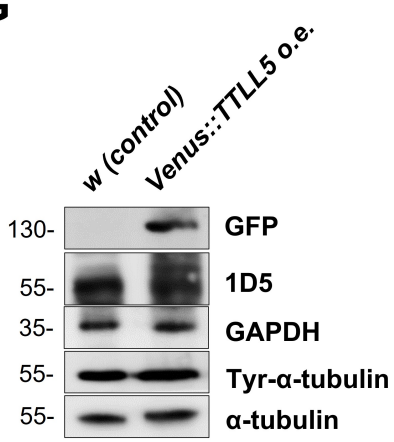

Fig. 4

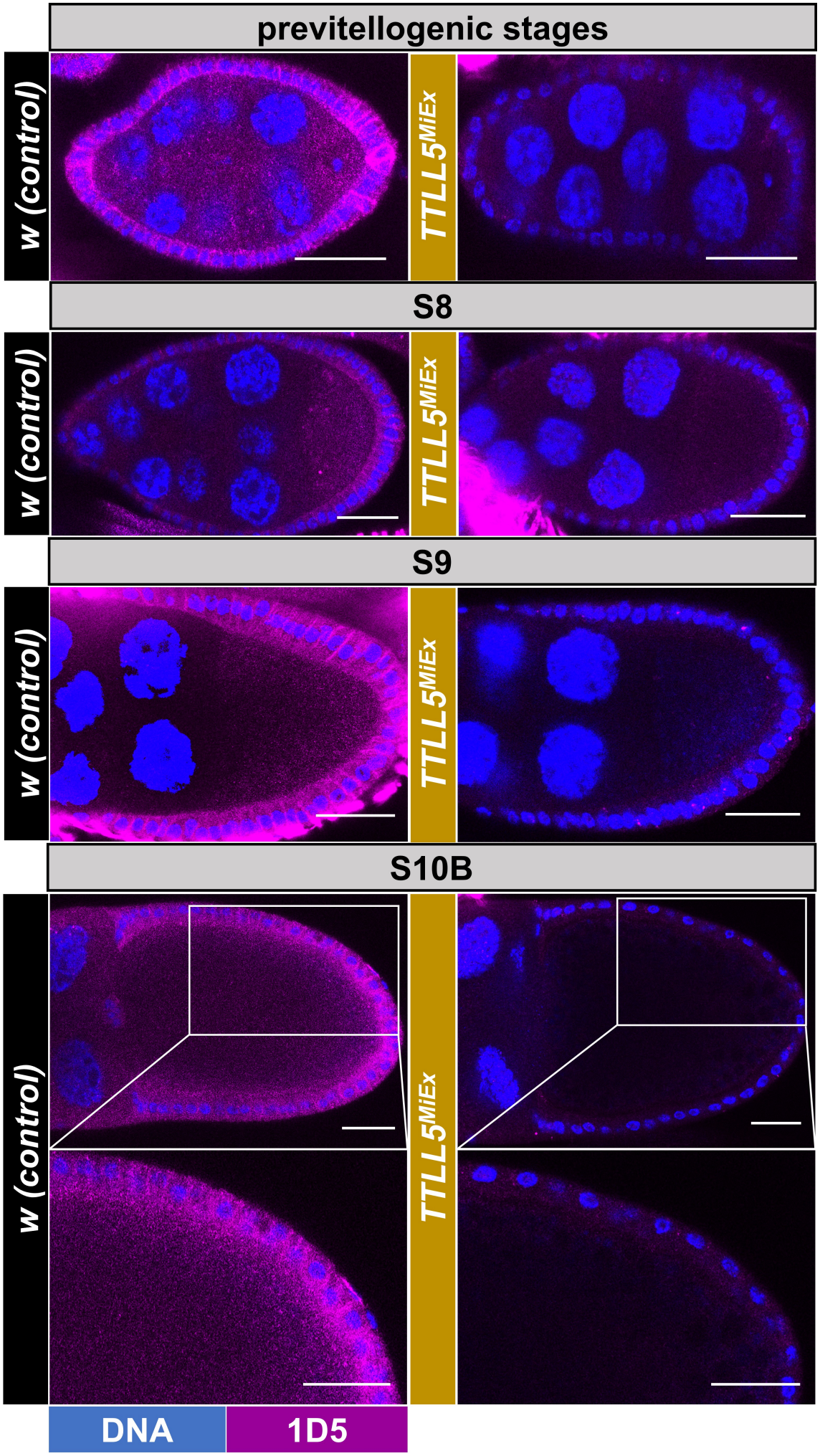
previtellogenic stages
S8
S9
S10B
w (control)
TTLL5MiEx
DNA
1D5

Fig. 5

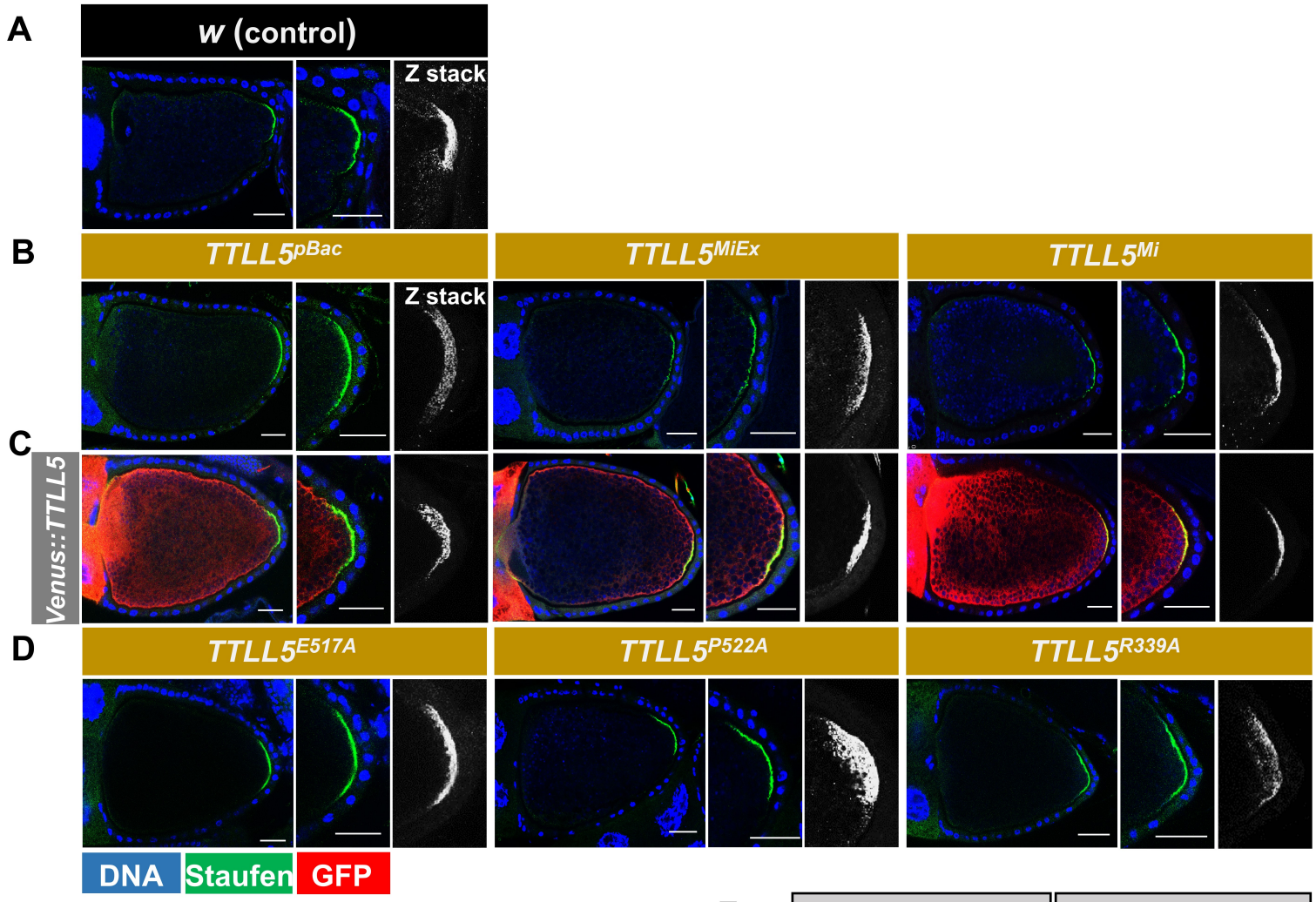
A
w (control)
Z stack
B
TTLL5pBac
TTLL5MiEx
TTLL5Mi
Z stack
C
Venus::TTLL5
D
TTLL5E517A
TTLL5P522A
TTLL5R339A
DNA
Staufen
GFP

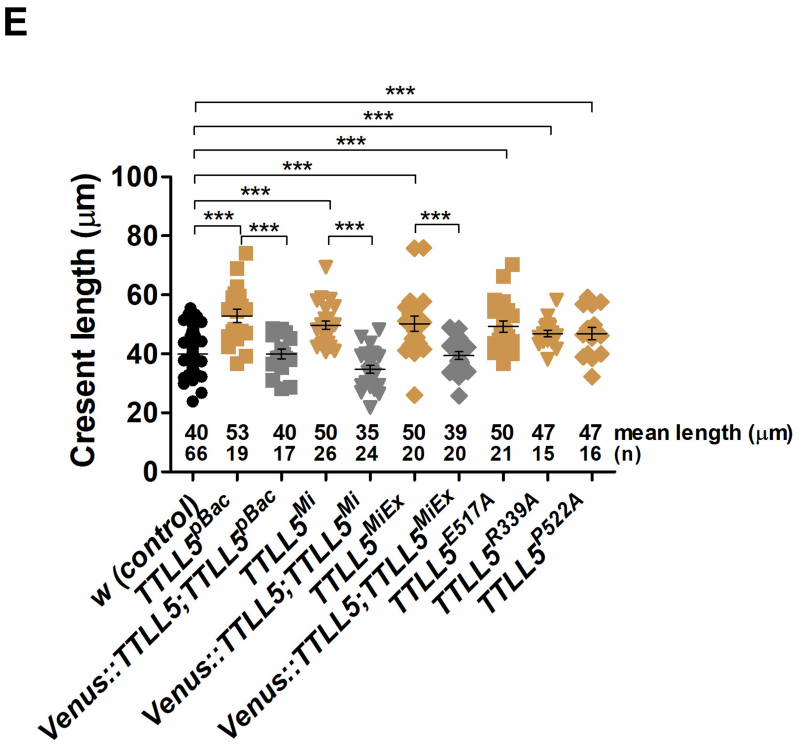
E
Cresent length (μm)
100
80
60
40
20
0
***
40 53 40 50 35 50 39 50 47 47 mean length (μm)
66 19 17 26 24 20 20 21 15 16 (n)
w (control)
TTLL5pBac
Venus::TTLL5;TTLL5pBac
TTLL5Mi
Venus::TTLL5;TTLL5Mi
TTLL5MiEx
Venus::TTLL5;TTLL5MiEx
TTLL5E517A
TTLL5R339A
TTLL5P522A

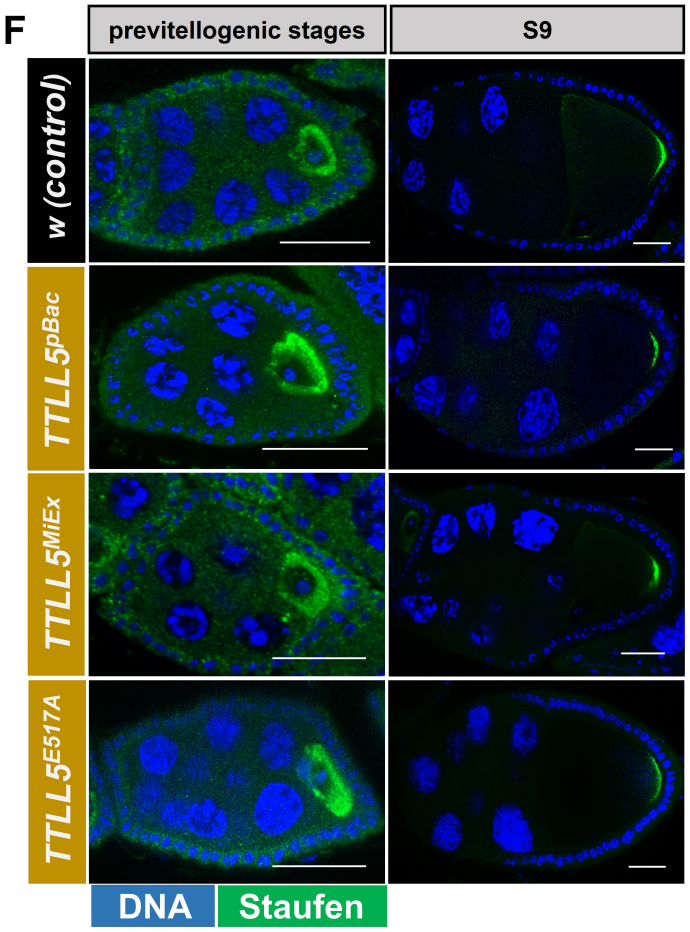
F
previtellogenic stages
S9
w (control)
TTLL5pBac
TTLL5MiEx
TTLL5E517A
DNA
Staufen

Fig. 6

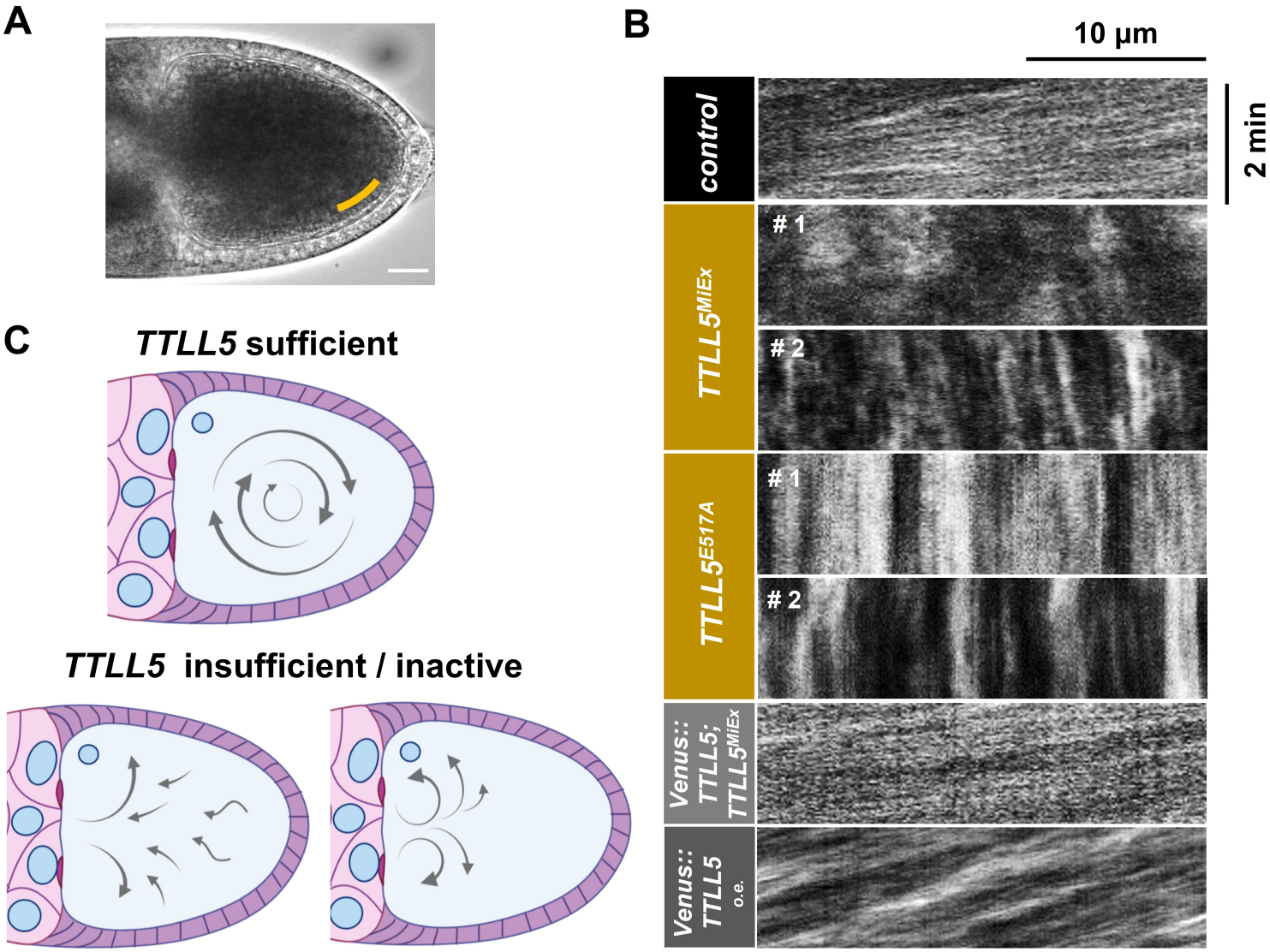
A
B
C
10 µm
2 min
control
TTLL5MiEx
1
2
TTLL5E517A
1
2
Venus::
TTLL5;
TTLL5MiEx
Venus::
TTLL5
o.e.
TTLL5 sufficient
TTLL5 insufficient / inactive

Fig. 7

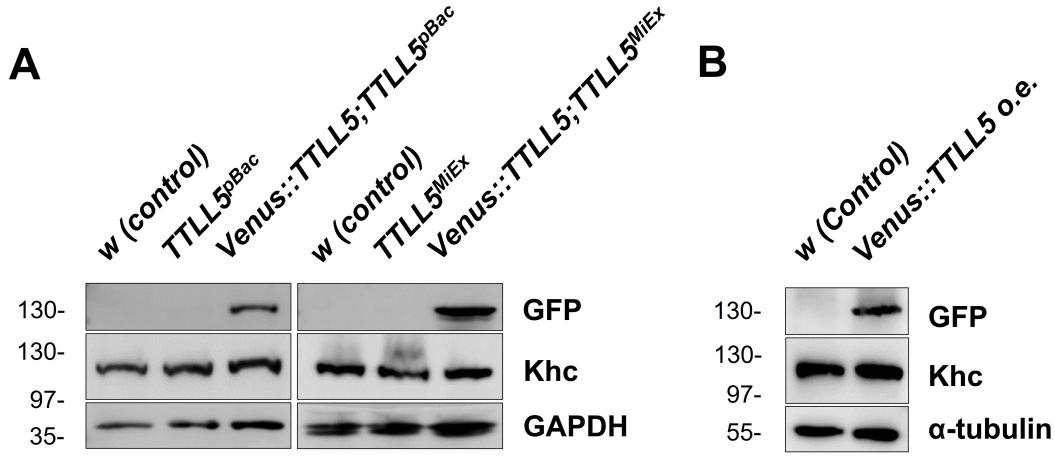
A
w (control)
TTLL5pBac
Venus::TTLL5;TTLL5pBac
w (control)
TTLL5MiEx
Venus::TTLL5;TTLL5MiEx
130-
130-
97-
35-
GFP
Khc
GAPDH
B
w (Control)
Venus::TTLL5 o.e.
130-
130-
97-
55-
GFP
Khc
α-tubulin

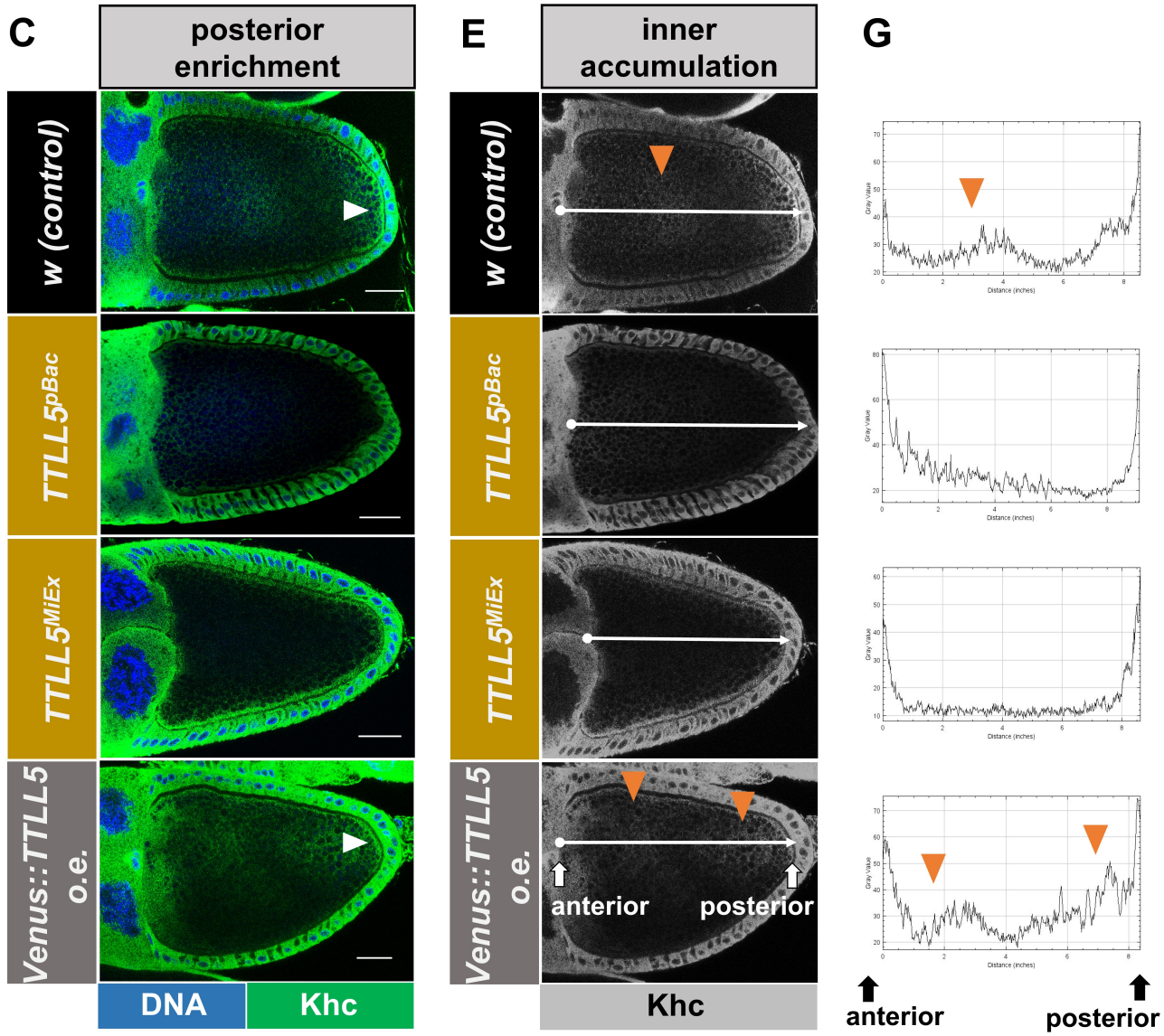
C
posterior enrichment
w (control)
TTLL5pBac
TTLL5MiEx
Venus::TTLL5 o.e.
DNA
Khc
E
inner accumulation
w (control)
TTLL5pBac
TTLL5MiEx
Venus::TTLL5 o.e.
anterior
posterior
Khc
G
anterior
posterior

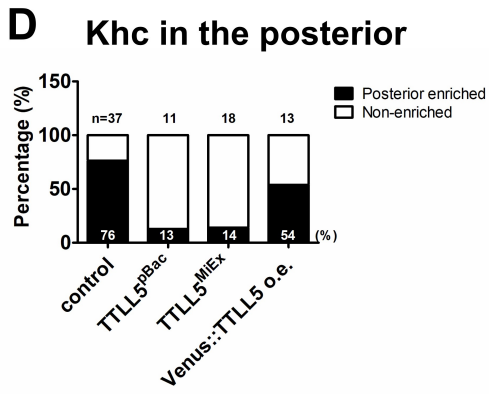
D
Khc in the posterior
Percentage (%)
150
100
50
0
n=37
11
18
13
76
13
14
54
(%)
Posterior enriched
Non-enriched
control
TTLL5pBac
TTLL5MiEx
Venus::TTLL5 o.e.

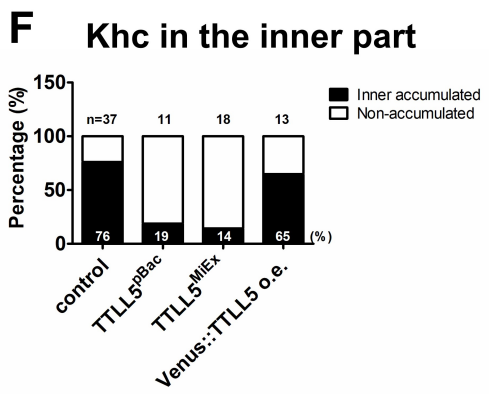
F
Khc in the inner part
Percentage (%)
150
100
50
0
n=37
11
18
13
76
19
14
65
(%)
Inner accumulated
Non-accumulated
control
TTLL5pBac
TTLL5MiEx
Venus::TTLL5 o.e.

Fig. 8

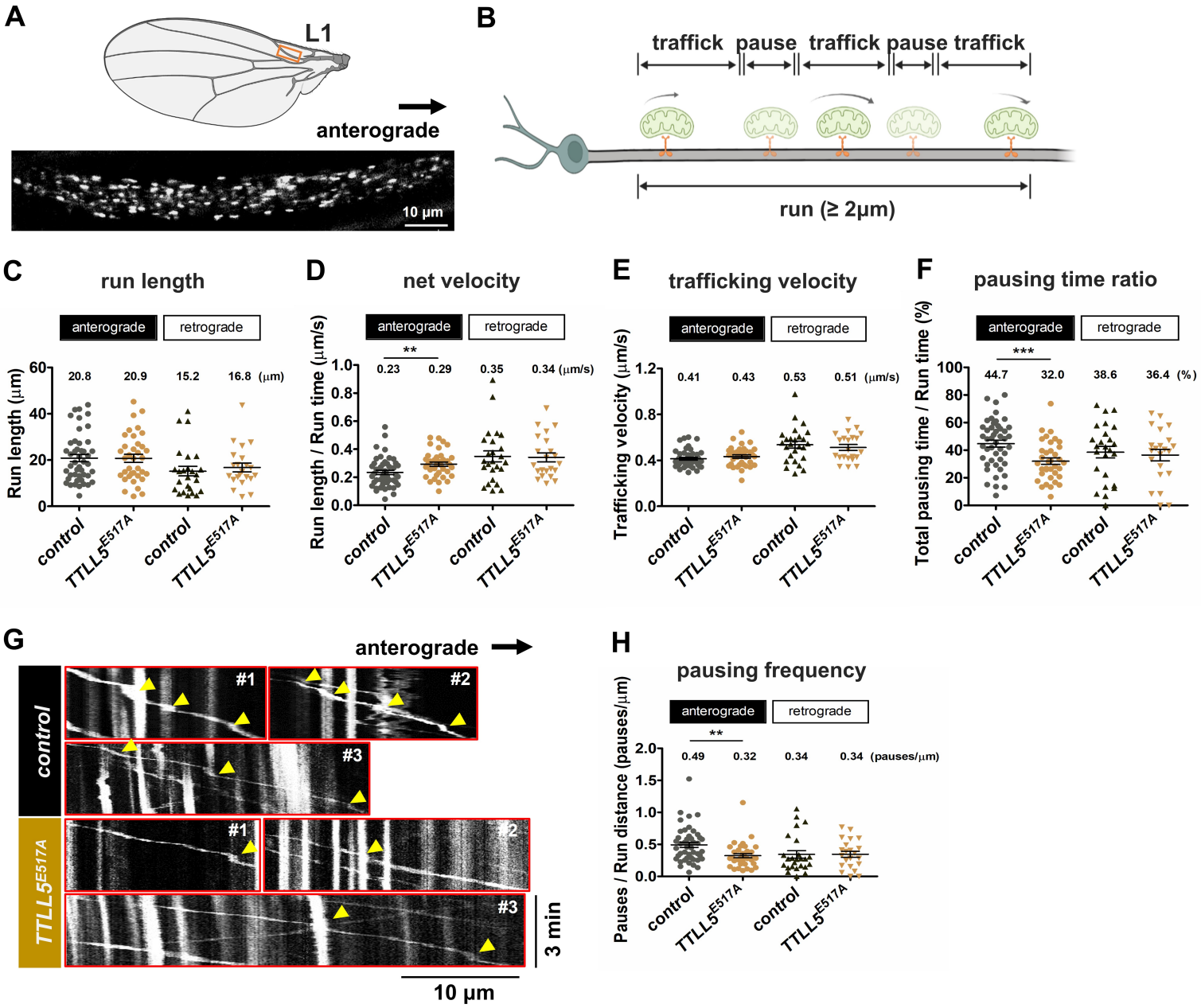
A
L1
anterograde
10 µm
B
traffick pause traffick pause traffick
run (≥ 2µm)
C
run length
anterograde
retrograde
Run length (µm)
20.8 20.9 15.2 16.8 (µm)
control
TTLL5E517A
D
net velocity
Run length / Run time (µm/s)
**
0.23 0.29 0.35 0.34 (µm/s)
E
trafficking velocity
Trafficking velocity (µm/s)
0.41 0.43 0.53 0.51 (µm/s)
F
pausing time ratio
Total pausing time / Run time (%)
***
44.7 32.0 38.6 36.4 (%)
G
anterograde
control
TTLL5E517A
#1
#2
#3
3 min
10 µm
H
pausing frequency
Pauses / Run distance (pauses/µm)
**
0.49 0.32 0.34 0.34 (pauses/µm)